Ore Geology Reviews 124 (2020) 103603

Contents lists available at ScienceDirect

Ore Geology Reviews

journal homepage: www.elsevier.com/locate/oregeorev

Geological, geophysical, and geochemical characteristics of the Ban Kiouchep Cu–Pb–Ag deposit and its exploration significance in Northern Laos

Haijun Zou[a,b,*], Runsheng Han[c], Mengqiong Liu[d], Paul Cromie[e], Khin Zaw[e], Weixuan Fang[f], Jianguo Huang[c], Tao Ren[c], Jin Wu[g]

[a] School of Resources and Environmental Engineering, Guizhou Institute of Technology, Guiyang 550003, China
[b] State Key Laboratory of Ore Deposit Geochemistry, Institute of Geochemistry, Chinese Academy of Science, Guiyang 550081, China
[c] Faculty of Land and Resources Engineering, Kunming University of Science and Technology, Kunming 650093, China
[d] Yunnan Provincial Architectural Engineering Design Institute, Kunming 650021, China
[e] CODES Centre of Ore Deposits and Earth Sciences, University of Tasmania, Private Bag 126, Hobart, Tasmania 7001, Australia
[f] Geological Survey Center for Non-ferrous Mineral Resources, Beijing 100012, China
[g] Yunnan Copper Industry (Group), Kunming 650051, China

ARTICLE INFO

Keywords:
Hydrothermal deposit
Oxidation leaching
Lateritization
Ban Kiouchep Cu–Pb–Ag deposit
Simao–Indochina Basin
Northern Laos

ABSTRACT

The Simao–Indochina Basin is located between the Loei–Luang Prabang–Dien Bien Phu fold belt and the Jinghong–Nan-Uttaradit suture zone, composed of Mesozoic and Cenozoic red beds. It overlies the marine clastic rocks and volcanic sedimentary rocks of a Paleozoic back-arc foreland sequence. The Late Triassic Indosinian orogeny and subsequent superimposition and intracontinental shearing and structural superimposition may have facilitated the formation of various deposits in this basin, including hydrothermal, skarn, and porphyry types of mineralization. The Ban Kiouchep Cu–Pb–Ag deposit is a medium–low-temperature hydrothermal deposit that is largely controlled by faults and is hosted in carbonate rocks and volcanic (-sedimentary) rocks. The formation of this deposit includes a series of geological and metallogenic processes (i) neritic–littoral facies (volcanic-) sedimentation in a Late Paleozoic to Late Triassic back-arc foreland setting, (ii) Indosinian orogenic transformation, (iii) Mesozoic–Cenozoic tectonic-hydrothermal overprinting, and (iv) epigenetic oxidized leaching. The ore minerals are primarily malachite, azurite, and galena, followed by sphalerite, chalcocite, and chalcopyrite, with associated silver minerals. Using induced polarization (IP) geophysical surveys and soil geochemical surveys, large-scale and highly overlapping coincident anomalies and a mineralized zone at a scale of 100–110-m size (ore body I) was discovered in the area. Two anomalies, P1-C1 and P5-C4, with the best metallogenic conditions and the deepest extensions of the known ore bodies, were further selected as engineering verification targets. The two following verifying drill holes revealed Pb–Zn–Ag mineralization in the fault zone; however, no mineralized ore bodies consistent with the anomalies were found. The high background value of the Fe–Cu–Pb–Zn (Ag) elements, strong fracturing, and hydrothermal alteration, as well as later oxidized leaching with lateritization, resulted in in-situ dispersion and local secondary enrichment of the metallogenic elements. These may be the primary causes of the overlapping anomaly distribution along the strata and faults therein. Lateritic Ag mineralization has been also found in the area. The geological, geophysical, and geochemical characteristics and the prospecting are of great importance for further research and prospecting for other related deposits, for example, the VHMS, SEDEX, hydrothermal Cu polymetallic deposits and porphyry, skarn, epithermal, sediment-hosted/orogenic Au deposits, with lateritic Ag (Au) deposits in the Simao–Indochina Basin of Northern Laos.

1. Introduction

Northern Laos and its adjacent terranes contain several tectonic units and host many types of important deposits with great exploration potential (e.g., Khin Zaw et al., 2014; Zhang et al., 2012; Wang et al., 2014; Wang and Shi, 2016; Hu et al., 2013). Generally, there are hydrothermal, skarn, and porphyry-related Cu–Au polymetallic mineralization and sediment-hosted/orogenic Au deposits in or near suture

* Corresponding author at: School of Resources and Environmental Engineering, Guizhou Institute of Technology, Guiyang 550003, China.
E-mail address: zouhaijun@git.edu.cn (H. Zou).

https://doi.org/10.1016/j.oregeorev.2020.103603
Received 28 March 2019; Received in revised form 13 May 2020; Accepted 21 May 2020
Available online 30 May 2020
0169-1368/

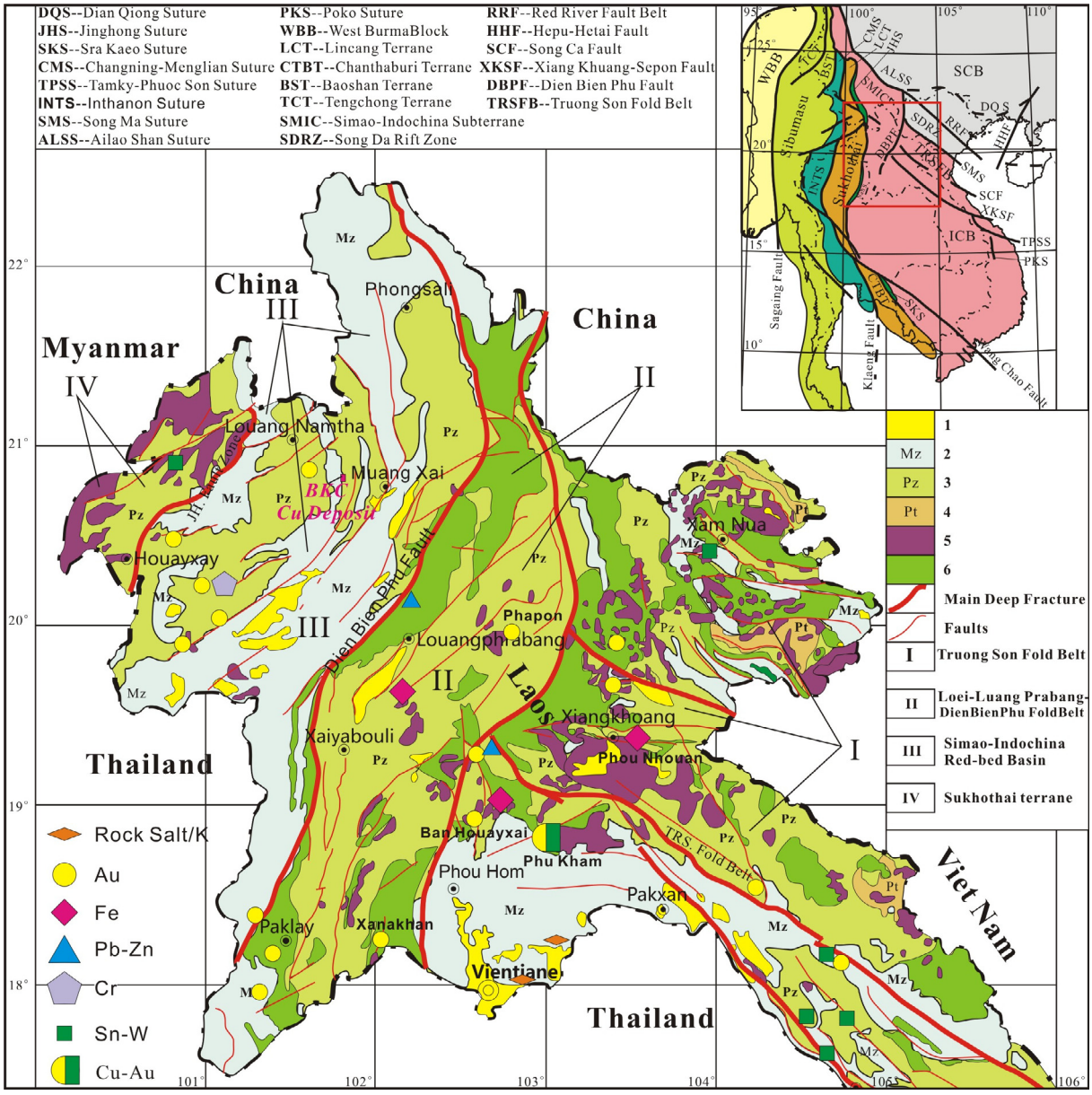

Fig. 1. Geological map of Northern Laos showing the tectonics and magmatic rocks and deposits: 1–Quaternary; 2–Mesozoic continental clastic rocks and intermediate-felsic volcanic rocks; 3–Paleozoic marine clastic rocks and intermediate-felsic volcanic rocks; 4–Precambrian gneisses and schists; 5–Granitoids; and 6–Volcanic complexes (modified from the Jia et al., 2014; Wang et al., 2016; ore deposits after Fan, 2000; tectonic framework plot of the Southeast Asia mainland after Metcalfe, 2013; Sone and Metcalfe, 2008; Wang et al., 2016).

zones among these terranes and intra-block fold belts (Kamvong et al., 2014; Goldfarb et al., 2014; Khin Zaw et al., 2014), such as the Phu Kham (Kamvong et al., 2014), Sepon (Manini et al., 2001; Smith et al., 2005; Cromie, 2010; Cromie et al., 2018), Selinsing, Tersang and Penjom deposits (Makoundi et al., 2014; Khin Zaw et al., 2014). However, geological and ore research and exploration work around this area are still lacking and studies focused on the division of the tectonic units and metallogenic belts (e.g., Cheng et al., 2011; Shi et al., 2013; Jia et al., 2014; Shao et al., 2015; Zhao et al., 2015; Gao et al., 2017). Therefore, in these poorly explored areas, it is necessary to investigate the use of integrated exploration methods to assist the discovery of resources. This paper provides geological, geophysical and geochemical exploration, and engineering investigation of the Ban Kiouchep Cu–Pb–Ag deposit and its exploration significance in Northern Laos.

The Mesozoic–Cenozoic Simao–Indochina red bed Basin (SM-IC Basin) is situated between the Loei–Luang Prabang–Dien Bien Phu Fold Belt (L-L-DBPFB; Lepvrier et al., 2004) and Jinghong–Nan-Uttaradit suture zone (JNU; exhumed back-arc basin) (Metcalfe, 2002, 2013; Lepvrier et al., 2004; Yan et al., 2006; Sone and Metcalfe, 2008; Faure et al., 2014) (Fig. 1). The Ban Kiouchep Cu–Pb–Ag deposit (BKC deposit) is located near the Ban Kiouchep Village in Namor County, Udomxay Province, Northern Laos (Fig. 1), and it is structurally controlled by faults and hosted in upper Triassic marine carbonate rocks. Geotectonically, the BKC deposit lies to the south of the SM-IC Basin (Feng et al., 2005), within the eastern Tethyan tectonic domain. The subsidiaries of the Yunnan Copper Industry Group have performed geological mapping, geochemical and induced polarization (IP) surveys (IP sounding) around the BKC deposit area. Furthermore, some trenches and pits, as well as two drill holes, have been completed in the deposit area. In addition, some researchers from Kunming University of Science and Technology have briefly studied the metallogenic features of the deposit. However, the understanding of the ore system is not sufficient to constrain the ore genesis, the relationship between the geophysical–geochemical anomalies and the lateritization, as well as the

connection with the regional tectono-magmatic-metallogenic processes.

Under the tectonic-magmatic evolution and mineralization processes in various tectonic units of northern Laos, the geological characteristics, tectonic-hydrothermal mineralization, and the laterite Ag mineralization information in the BKC deposit are investigated in this contribution through prospecting and exploration program. This work provides guideline and significant information for the mineral prospecting and an in-depth study of the related types of deposits in the SM-IC Basin and adjacent areas in Northern Laos.

2. Regional geological framework

2.1. Tectonic setting

The Southeast Asian continent is an accretion of multiple terranes (e.g., Fan, 2000; Acharyya, 2000; Sone and Metcalfe, 2008; Metcalfe, 2002, 2013; Khin Zaw et al., 2014) and is primarily comprising the Simao–Indochina Block (SM-ICB), the Northern Vietnam terrane (of South China Block, SCB), and the Sibumasu Block (SBMS), West Burma, and Northwest Borneo (Semitau) terranes (Metcalfe, 2002; Merdith et al., 2017) (Fig. 1), bounded by sutures or fold zones (Sone and Metcalfe, 2008; Metcalfe, 2002, 2013; Qian et al, 2015; Lepvrier et al., 2004; Yan et al., 2006; Roger et al., 2014; Wang et al., 2016; Bui et al., 2017; Fan et al., 2010; Liu et al., 2015, 2017; Domeier and Torsvik, 2014; Deng et al., 2015; Xia et al., 2016; Faure et al., 2017; Zi et al., 2012; Acharyya, 1998; Thanh et al., 2011, 2014; Otofuji et al., 2012; Wang et al., 2014; Khin Zaw et al., 2014). These terranes drifted from Gondwana and moved northward through the opening and closing of the Paleo-Tethys Ocean during the Paleozoic and eventually converged via collisions in the Late Triassic Indosinian orogeny (Golonka, 2007; Deng and Wang, 2016; Li et al., 2018; Khin Zaw et al., 2014). This orogeny resulted in the Late Permian–Early and Middle Triassic collision between the SM-ICB and SCB, followed by the late Triassic collision between the SM-ICB and SBMS, as well as the Triassic–Cenozoic arc–continent (Sukhothai Arc and SM-ICB) and continent–continent collision/accretion (Khin Zaw et al., 2014; Zou et al., 2017). As a northern part of the Southeast Asia, Northern Laos occupies the junction of the subduction, the demise of the Paleo-Tethys Ocean, and the collision–accretion of the SCB, ICB, Sibumasu, and their accretionary terranes at different tectonic stages (Khin Zaw et al., 2014). Northern Laos belongs to the Tethyan tectonic domain on the SM-ICB (Fig. 1). From east to west, it successively spans the Truong Son fold belt (TS) (Manaka et al., 2014), the L-L-DBPFB (Lepvrier et al., 2004; Qian et al., 2015; Rossignol et al., 2016), the SM-IC Basin (Sone and Metcalfe, 2008; Wang et al., 2016), the JNU (Qian et al., 2015; Hou and Zhang, 2015; Tabakh and Utha-Aroon, 1998; Fan, 2000; Lepvrier et al., 2004; Wang et al., 2016; Yan et al., 2006), and the Sukhothai Arc (SKTA) (Bunopas et al., 2001; Goldfarb et al., 2014) (Fig. 1; Table 1).

The SM-IC Basin developed on the marine sedimentary base of a Paleozoic back-arc foreland basin on the western margin of SM-ICB (Fig. 1). It was uplifted by the late Triassic Indosinian orogeny, accepting fold belt sediments from north, northeast, and west. From the Mesozoic on, this area evolved into a terrestrial red bed basin, forming cover strata, and was subjected to imprinting and intracontinental shearing due to the Mesozoic regional tectono-magmatic activities and the continental collision of the Cenozoic Himalayan movement (Zhang et al., 1999; Acharyya, 2000; Wang et al., 2001; Yin, 2010; Morley, 2002).

The regional structures extend in NNW or NE–SW direction to the north and in NE–SW trend to the south (Fig. 1; Fig. 2d). The SM-IC Basin is bounded by the NW-trending Ailaoshan–Song Ma tectonic belt to the northeast, with the NE-trending JNU to the northwest and the L-L-DBPFB to the east. The nearly S–N-trending Lancangjiang (Mekong River) fault passes through the western part of the area (Fig. 1). The left-lateral strike-slip regime of the large regional tectonic belts resulted in continuous compressive stress effects on the E–W and NE–SW-trending structures, forming a series of folds and faults as supporting structures and reforming the structural frame of the SM-IC Basin, including the BCK deposit area (Fig. 1; Fig. 2b and 2c).

2.2. Stratigraphic setting

The Paleozoic strata in the SM-IC Basin are comprised of intermediate–felsic volcanic rocks (metamorphic marine volcanic-sedimentary rock series) and marine clastic rocks (sandstone, mudstone, shale, and limestone) (Zhao et al., 2013; Jia et al., 2014). The Mesozoic strata consist of marine and continental clastic rocks (sandstone, clay, mudstone, and limestone), with intermediate-felsic volcanic rocks, and the Cenozoic strata are primarily composed of conglomerate, sandstone, shale, siltstone, volcanic ash and lignite (Jia et al., 2014).

2.3. Magmatism

Regionally, the Indosinian granites are primarily distributed in the JNU to the west of the SM-IC Basin and in the L-L-DBPFB to the east (Fig. 1) and are only sporadically exposed in the inner basin. Paleozoic volcanic complexes are interbedded with synchronous sedimentary formations, primarily occurring in the L-L-DBPFB and continuously along the NE–SW-trending east side of the basin (Fig. 1). The magmatism in the basin was not strong, and only a small quantity of volcanic-clastic rocks and lava formed via volcanic eruptions can be a record of the Triassic volcanic activity. For example, gray carbonate-altered, sericite andesite tuffaceous rocks and gray altered layered intermediate–mafic tuffaceous sandstones have been found in the northwestern part of the BKC deposit. They show unidirectionally distributed and laminated volcanic debris interbedded with volcanic ash. The volcanic rocks consist of mafic, to felsic tuffaceous materials, probably formed by a volcanic eruption under sub-marine conditions. A drill hole exposed a yellowish-brown semi-weathered andesite body (Middlemost, 1972) in the ore-hosting strata, suggesting that the exhumation of the Paleozoic back-arc foreland basin may have begun in the Late Triassic due to the Indosinian orogeny.

2.4. Mineral resources in tectonic units of Northern Laos

Since the Paleozoic, Northern Laos and its extended tectonic units have undergone complex tectono-magmatic evolution and associated mineralization related to the development of the Tethyan tectonic domain, including several stages of ocean–continent subduction, island arc volcanism, back-arc basin sedimentation, arc–continent collision, post-collisional extension and terrigenous sedimentation. Moreover, volcanic–magmatic activities in the fold belts, back-arc basins, and continental margin arcs resulted in the magmatic–hydrothermal processes and mineralization on both sides of the region (Table 1). This tectonic and magmatic activities provided abundant circulation of metallogenic fluids and elements for mixing with upper crustal ore-forming materials to form hydrothermal, skarn, and porphyry-related Cu–Au and epithermal Au mineralization, sediment-hosted/orogenic Au deposits in the area and the adjacent regions (Table 1) (Khin Zaw et al., 2014; Kamvong et al., 2014; Goldfarb et al., 2014).

For example, the closure of the Nan–Sra Kaeo back-arc basin (i.e. JNU) generated the Loei continental margin arc magmatism (Khin Zaw et al., 2014). The L-L-DBPFB controls such magmatism and associated epithermal Au mineralization (e.g., Chatree, Wang Yai and Ban Houayxai deposits), skarn-type mineralization (e.g. Puthep and Phu Thap Fah deposits) and porphyry-related Cu-Au mineralization on both sides (Khin Zaw et al., 2014; Goldfarb et al., 2014). The magmatic process also produced adakitic–calcalkaline volcanic-plutonic rocks resulting in magmatic–hydrothermal fluids to porphyry Cu-Au deposits along the belt (Table 1) (Kamvong et al., 2014). Relatively, under regional tectonic–hydrothermal activities, various types of mineralization have also occurred in the SM-IC Basin (Table 1), including formation of:

Table 1
Tectonic units and metallogenic specialization in Northern Laos.

Tectonic Units	Attribute	Lithology	Ages	Metallogeny	Important Ore-deposits	References
L-L-DBPFB (Loei–Luang Prabang–Dien Bien Phu Fold Belt)	Plutonic volcanic arc/intra-continental magmatic arc	Andesite-rhyolite volcanic complexes (basalt, basalt andesite, dacite, volcanic clastic, andesite-dacite tuff; Adakite (Puthep 1 and 2, Thailand); Granite complex (north and south)	Early Carboniferous- Late Permian- Triassic Volcanic rock 150–350 Ma; Intrusive rock 256–340 Ma	(a) Tectonic-magmatic related porphyry, skarn, low-temperature hydrothermal Cu, Sn, Pb, Zn, Au, Sb and other deposits; (b) Sediment hosted/orogenic Au deposits; (c) Placer Au deposits	Epithermal Au Deposits: Chatree, Long Chieng Track, Phu He, Phapon, Paklay, Pangkham, Xanakhan; Skarn deposits: Phu Lon Cu-Au Puthep Cu-Fe, Phu Thap Fah Au	Sangsomphong et al., 2015; Salam et al., 2014; Lepvrier et al., 2004; Rossignol et al., 2016; Khin Zaw et al., 2014; Tabakh and Utha-Aroon, 1998; Goldfarb et al., 2014; Wang et al., 2016; Kamvong and Zaw, 2009; Manaka et al., 2014; Kamvong et al., 2014; Qian et al., 2015; Zhang et al., 2012
SM-IC Basin (Simao–Indochina red bed Basin)	Paleozoic back-arc foreland basin; Meso- Cenozoic continental red-bed basin	Late Permian ~ Late Triassic: marine carbonates, clastic rocks, andesite tuffs, andesite-dacite tuffs, sodic crystal tuffs; Jurassic-Cretaceous continental red clastic rocks	Late Permian-Mesozoic-Cenozoic	(a) Terrestrial sedimentary diagenesis-remobilized metallogeny related stratiform sandstone-type and structurally controlled hydrothermal veined Cu (Pb, Ag) polymetallic deposits; (b) Evaporite type gypsum-salt deposits; (c) Coal; (d) Triassic sedimentary- remobilized Fe, Cu and Mn deposits; (e) Laterite-type Au, Ag deposits; (f) Placer Au deposits	Jinding strata-bound Zn–Pb–Ag deposit, Nanpo and Ban Sinchai Sandstone-type Cu deposit, Mengla Xinshan Triassic Cu-Fe Deposit, Ban Namor and Phu Thung Late Triassic Cu deposits	Lepvrier et al., 2004; Yan et al., 2006; Roger et al, 2014; Bui et al., 2017; Liu et al., 2015, 2017; Metcalfe, 2002, 2013; Huang et al., 2019; Zi et al., 2012; Deng et al., 2015; Deng and Wang, 2016; Khin Zaw et al., 2007; Lai et al., 2012; Huang and Opdyke, 2016; Faure et al., 2017; Domeier and Torsvik, 2014; Tabakh and Utha-Aroon, 1998; Sone and Metcalfe, 2008; Thanh et al., 2011, 2014; Fan, 2000; Wang et al., 2014; Acharyya, 1998; Wang et al., 2016; Li et al., 2018; Fan et al., 2010; Xia et al., 2016; Otofuji et al., 2012; Zhao et al., 2015
JNU (Jinghong–Nan-Uttaradit suture zone)	Folded back arc basin	Paleozoic basic-ultramafic ophiolite (peridotite, metadiabase, amphibolite)/arc volcanic rocks and greywacke; diabase and coarse-grained basalt (Luang Prabang area); Late Paleozoic marine sedimentary rocks, volcanic complex, volcanic sedimentary rocks, metasedimentary rocks and granite	Carboniferous- Early Triassic (or Middle Devonian-Middle Triassic); 335.5 ± 3.3 Ma, 304.9 ± 3.9 Ma (Luang Prabang diabase and coarse-grained basalt)	(a) VHMS type Cu and SEDEX type Cu-Pb-Zn polymetallic deposits; (b) Volcanic sedimentary-remobilized Fe, Cu, Pb, Zn, Au, Ag deposit; (c) Hydrothermal Cu, Au, Pb, Ag, Sb deposits related to regional tectonic activities or intermediate-acid magmatism; (d) laterite type Ag (Au, Cu, Pb, Zn) deposits	Triassic Sandashan Cu deposit in Jinghong; Dapingzhang Late Carboniferous Cu–Zn type VHMS deposit	Lepvrier et al., 2004; Yan et al., 2006; Metcalfe, 2002, 2013 ; Khin Zaw et al., 2007, 2014; Tabakh and Utha-Aroon, 1998; Sone and Metcalfe, 2008; Faure et al., 2014; Domeier and Torsvik, 2014; Thanh et al., 2011, 2014; Ferrari et al., 2008; Fan, 2000; Wang et al., 2016; Acharyya, 1998; Qian et al., 2015, 2016; Otofuji et al., 2012; Hou and Zhang, 2015
Sukhothai Arc (SKTA)	Volcanic island arc system	Shallow-marine sedimentary rocks and igneous rocks with I-type granitoids (Sukhothai Terrane/Arc, Inthanon Suture Zone, Chanthaburi Pluton), Lincang granitoids	Permian and Triassic; 210 Ma for Chanthaburi Pluton; 280–210 Ma for Lincang granitoids	(a) Au and gemstone deposits related to basic ultrabasic volcanic activity; (b) Porphyry, skarn, hydrothermal Cu, Au, Fe, Pb, Zn, Sn, Sb deposits related to intermediate-acid magmatic intrusions and relevant hydrothermal activities.	Ban Houayxay, Ban Huai Sai Corundum plus spinel group	Lepvrier et al., 2004; Dill and Weber, 2013; Metcalfe, 2013; Domeier and Torsvik, 2014; Sone and Metcalfe, 2008; Goldfarb et al., 2014; Bunopas et al., 2001; Qian et al., 2015

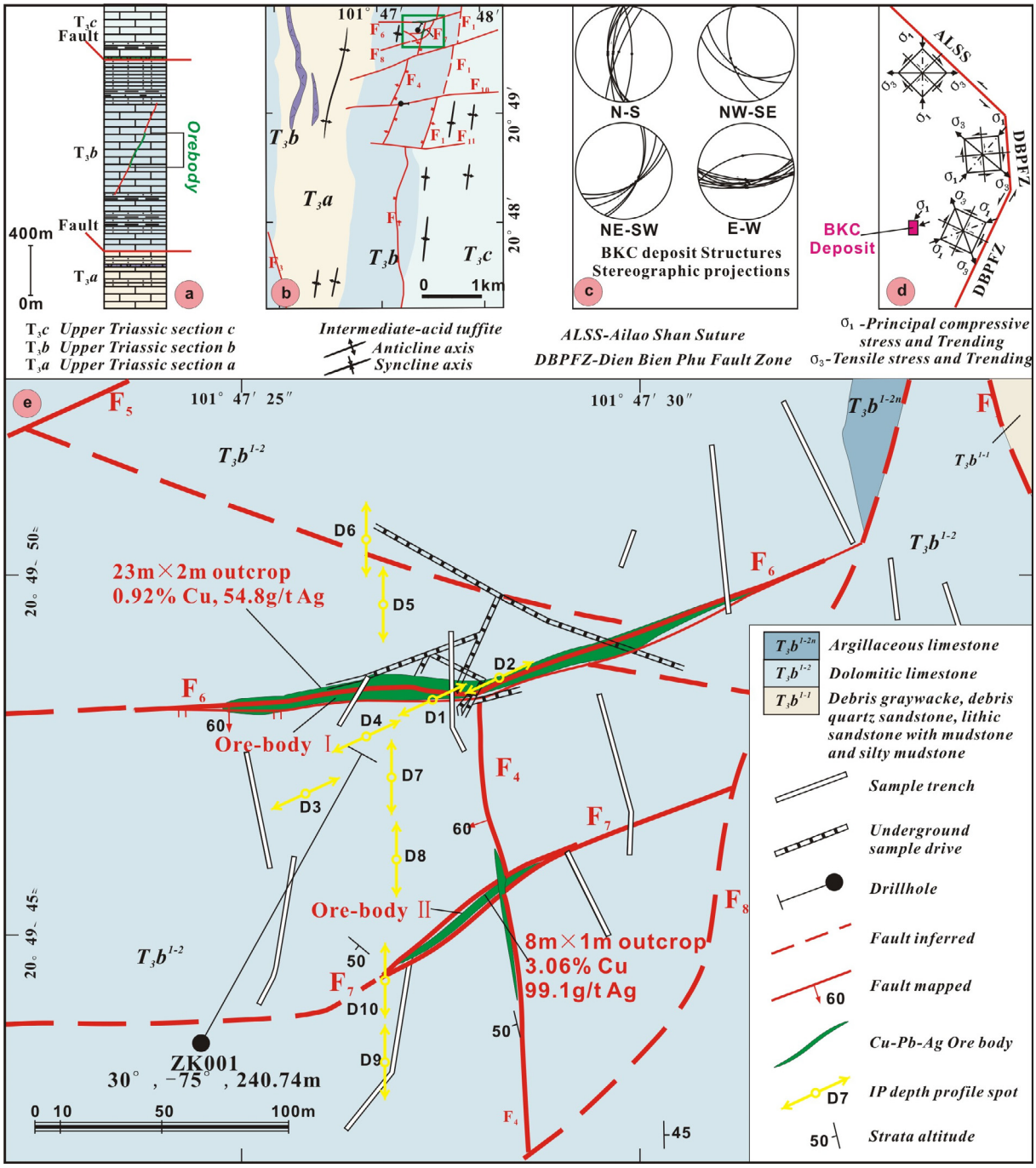

Fig. 2. District–deposit-scale geological map of the BKC Cu–Pb–Ag deposit, Northern Laos: (a) sedimentary sequences; (b) district-scale structures; (c) structural stereographic projections of the BKC deposit (S hammer sphere, equal area); (d) regional tectonic stress analysis sketch; and (e) the BKC deposit-scale geology.

the Cu–Fe–Au and Mn polymetallic deposits related to the Permian–late Triassic volcanism and sedimentation (e.g., Yunnan–Luang Namtha–-Luang Prabang area), as well as the stratiform sandstone-type Cu deposits related to the Jurassic–Cretaceous (J-K) terrestrial clastic sedimentation (e.g., Yunnan–Phongsaly–Udomxay area), and fault controlled Cu–Pb–Ag polymetallic deposits hosted by carbonate-bearing late Triassic volcanic rocks (e.g., the Udomxay–Luang Prabang area). The deposits are also associated with the evaporite, gypsum, and salt rocks (potassium-bearing) deposits occurring in the Cretaceous–early Tertiary (K-E) red beds.

Consequently, northern Laos is an important target area for prospecting and the exploration of Au, Ag, Cu, Pb, Sn, W, Fe, Sb, and Hg, as well as non-metallic minerals such as coal, gypsum salt, and building materials (Fig. 1; Table 1). Important example deposits have been discovered (Table 1), involving the Phu Kham porphyry/skarn Cu–Au deposits, the LCT/Ban Houayxai hydrothermal Au deposit on the Troung Son belt (Khin Zaw et al., 2014; Manaka et al., 2014), Phu He (Goldfarb et al., 2014), Phapon (Zhang et al., 2012), Paklay Pangkham, and the Xanakhan hydrothermal (epithermal) Au deposits. The Phu Lon skarn Cu–Au deposit (Kamvong and Khin Zaw, 2009), the Puthep Cu–Fe skarn deposit and the Phu Thap Fah skarn Au deposits (Khin Zaw et al., 2007) and the Chatree epithermal Au deposit (Salam et al., 2014) occurred along the L-L-DBPFB. The SM-IC Basin is also consisted of the Jinding strata-bound Zn–Pb–Ag deposit (Khin Zaw et al., 2007), the Ban Sinchai and Nanpo sandstone-type Cu–Ag deposit (Huang et al., 2019), the Xinshan Triassic Cu–Fe–Pb–Zn deposit (Dai et al., 2016), the Ban

Namor and Phu Thung hydrothermal Cu deposits (Zhao et al., 2015) as well as, the Triassic-cupriferous Sandashan Cu deposit, the Dapingzhang late-Carboniferous VHMS Cu–Zn deposit (Khin Zaw et al., 2007) on the JNU, the Ban Houayxay (Ban Huai Sai) corundum plus spinel group (Dill and Weber, 2013), and sapphire deposit (Sutherland et al., 2002) on the Houayxay belt (of the SKTA).

3. Ore deposit geology

3.1. Geological characteristics

Through geological mapping, it is documented that only the upper Triassic and the littoral facies, intertidal zone (tidal flat), and shallow marine facies flysch sedimentation assemblages are commonly recorded. As the carbonate-variegated fine clastic rocks and intermediate–mafic, intermediate–felsic pyroclastic rocks, and intermediate–felsic tuffaceous rocks are exposed in the BKC deposit area; these sedimentary sequences are also rich in Tethyan fauna fossil groups (Fig. 2a). No intrusive rocks were found except for the gray intermediate–mafic tuffaceous rocks and andesite sandwiched in the Triassic strata.

The regional stratigraphic strikes and tectonic trends change from NNW or N–S-trending in the north to NE–SW-trending in the south of the area (Fig. 1 and Fig. 2d). The nearly N–S-trending faults are dominating the sedimentary strata and the structural setting in the BKC deposit area (Fig. 2b and 2c), forming a complex anticlinal structure with a nearly N–S axis and mostly S–N to NW–SE-trending secondary folds on its flanks. The nearly N–S-trending left-lateral compressive–-torsional folds and faults are appeared to be earlier stage structures, while the NW–SE-trending left-lateral torsional–compressive faults are formed in middle stage structures. The late stage structures are nearly E–W-trending large-scale right-lateral tensional–torsional faults and NE-trending right-lateral torsional strike-slip faults in this area (Fig. 2b and 2c).

The BKC Cu–Pb–Ag deposit occurred within the E–W-trending compressive–torsional fault belts and at an intersection with the N–S-trending faults (Fig. 2e). The E–W and NE-trending faults are ore-controlling and ore-hosting structures, and the Pb–Zn mineralization-associated wall-rock alteration, such as carbonatization and silicification and related chalcopyrite occurrence are common in the nearly N–S-trending fault zones.

In details, the BKC deposit consists of two Cu–Pb–Ag ore bodies, namely I and II, which are controlled by the nearly E–W-trending F_6 and F_7 faults, respectively. The ore-hosting rocks are primarily composed of gray–dark gray dolomitic limestone (Fig. 2e). The ores were further enriched via a secondary process and were recrystallized/reformed by faulting (e.g., at the intersection of faults F_7 and F_4).

The attitudes of the ore bodies I and II are consistent with the ore hosting fault zones: 43–120-m long along the strike, ~160-m deep, and 1–3-m thick on average. The ores range from 1.06 to 1.71% Cu, 72.2–99.14 g/t Ag, and up to 4.28% Pb. The ore minerals are mainly malachite, azurite, and galena, along with sphalerite, chalcopyrite, chalcocite, and associated silver minerals (Fig. 3). The gangue minerals are dolomite, calcite, and a small amount of quartz. The ores have shell-like, veinlet-disseminated, as well as massive structures and are poorly cemented. Pyrite, chalcopyrite, malachite, and azurite are main mineralization ores, whereas the wall rock alterations are primarily of carbonatization (carbonatization and calcitization) and limonitization with minor silicification (Zhou et al., 2014, 2018a, b, c). Galena-Sphalerite and azurite–malachite mineralization is dispersed in veinlets along the alteration zones showing uneven mineralization distribution (Fig. 3d). The wall rock alteration has a clear relationship with the fault and displays characteristics of decreasing intensity outwards from the fault and mineralization center.

3.2. A generalized mineralization model

Combined with the regional setting and the geological characteristics of the BKC deposit, including the mineralogy and textural relationships of the ore minerals, the paragenetic sequence is: pyrite + sphalerite + galena → pyrite + chalcopyrite → chalcocite + azurite + malachite + limonite (Fig. 4). The ore-forming process was probably initiated during the neritic–littoral facies sedimentation–diagenesis stage in a late Paleozoic–late Triassic back-arc foreland basin, followed by the Indosinian orogenic-metallogenetic stage, and the Mesozoic–Cenozoic superimposed–transformed mineralization stage, as well as by an epigenetic oxidation–leaching stage (Fig. 4). Therefore, we propose a conceptual mineralization model to describe its ore-forming process (Fig. 5): (i) During the late Paleozoic-late Triassic, neritic–littoral facies sedimentation in the back-arc foreland basin and intermediate–mafic volcanism and sedimentation were formed with high background contents of Cu, Pb, Zn, and Ag, and the rocks were dispersed with sulfides (e.g., pyrite and chalcopyrite). (ii) The Indosinian orogeny led to the formation of a continental red bed basin, while later tectonic–hydrothermal fluids extracted ore elements such as Cu from the strata and precipitated sulfide minerals (e.g., chalcopyrite and chalcocite) in the fault zones, primarily as vein-like and disseminated ores. The rocks near the fracture zones were deformed and broken up and then cemented together along the N–S-trending thrust faults which had provided the fluid channels for subsequent hydrothermal activity. (iii) Regional E–W-trending to NE–SW-trending compressive stresses resulted from the Mesozoic–Cenozoic tectonic extrusion movements and created a fracture-based conditions (e.g., a secondary distortion due to the NW-trending sinistral compressive–torsional faults, EW-trending dextral torsional–tensional faults, and NE-trending dextral torsional strike-slip faults), with hydrothermal superimposition. The ore-forming elements, such as Cu, Pb, Zn, and Ag in the strata containing volcanic sediments, were released with the ore-bearing hydrothermal fluids that migrated along the fault systems and were deposited and mineralized at the intersection of the N-S-trending and nearly E-W-trending fault zones (Fig. 2). (iv) Due to a low latitude climatic environment, the formed mineralization and ore-bearing strata were subjected to oxidation–leaching processes during strong weathering, forming oxidized ore bodies and laterite Ag–Fe–Cu anomalies predominated by minerals such as azurite, malachite, and limonite.

The Cu polymetallic mineralization is considered to be of neritic facies (volcanic–) sedimentary–reformed medium–low temperature hydrothermal type, controlled by faults (Fig. 2e and 5). In addition, it is characterized by the late Ediacaran–middle Permian carbonate-hosted and structurally controlled reverse fault–anticline epigenetic medium–low-temperature base metal deposits in the giant Upper Yangtze Pb–Zn province in SW China (Zhou et al., 2014, 2018a, b, c). The isotopic compositions suggest that ore-forming metals were locally sourced from the basement, sediments (carbonates), and volcanic rocks from which they mixed with multiple sulphur species-bearing, metal-rich fluids. Then, the ore fluids flowed through the favorable structures, they interacted with the host rocks and deposited, aided both by abiotic thermochemical and bacterially mediated processes, especially reacted with the organic matter-rich black shales within the compressional zones of the continental margin tectonic setting (Zhou et al., 2014, 2018a, b, c). This model provides new insights into the ore research and exploration of the BCK deposit and throughout the whole SM-IC Basin (Fig. 1).

4. Methods and results of the geophysical and geochemical survey

4.1. Geophysical and geochemical methods

Using the comprehensive and interdisciplinary methods involving geology, geophysics and geochemistry, further studies were performed

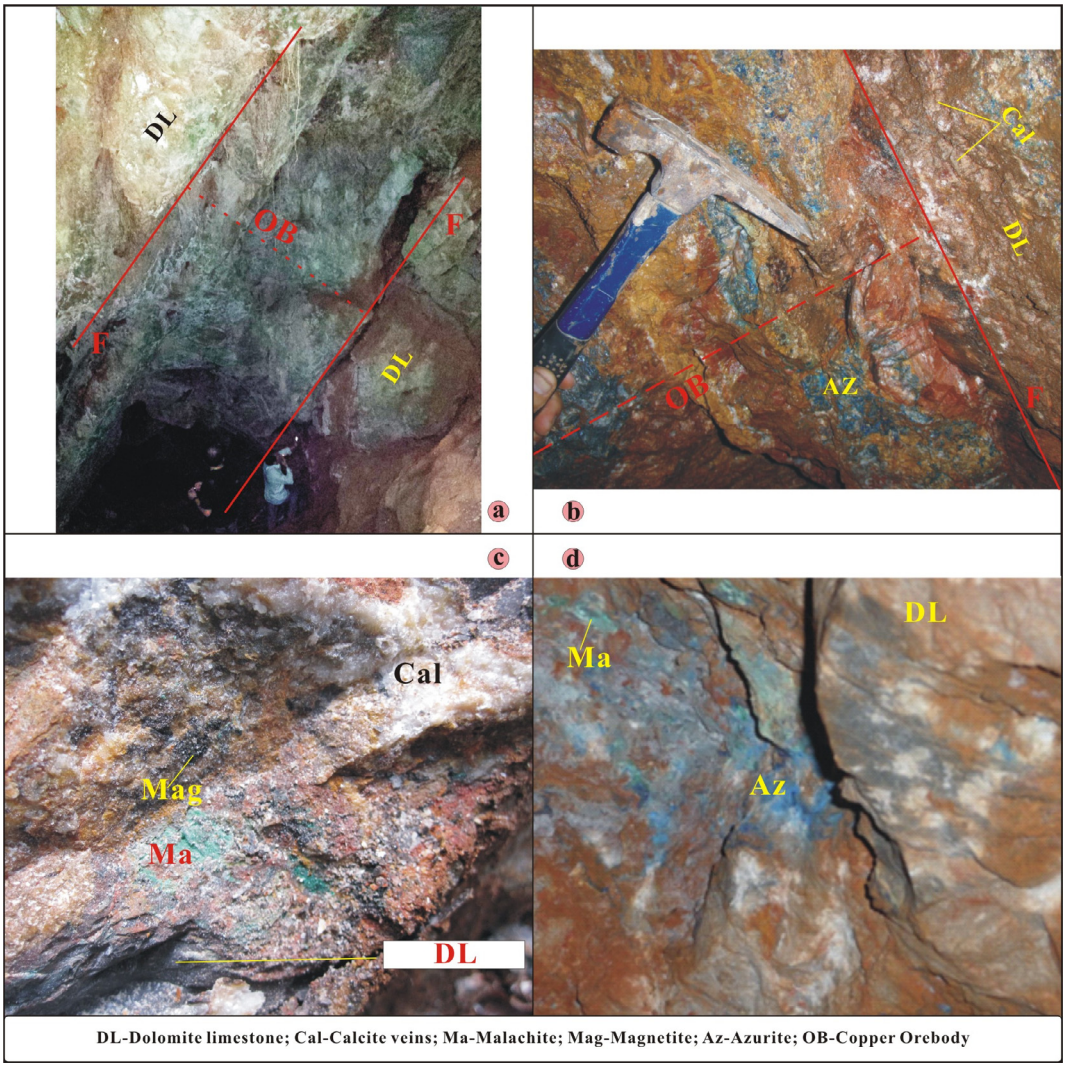

Fig. 3. Pictures showing the features of the ore bodies in the BKC Cu–Pb–Ag deposit, Northern Laos: (a), (b) ore body I; (c) ore body II; and (d) oxidized and leached copper mineralization in the T_3b limestone.

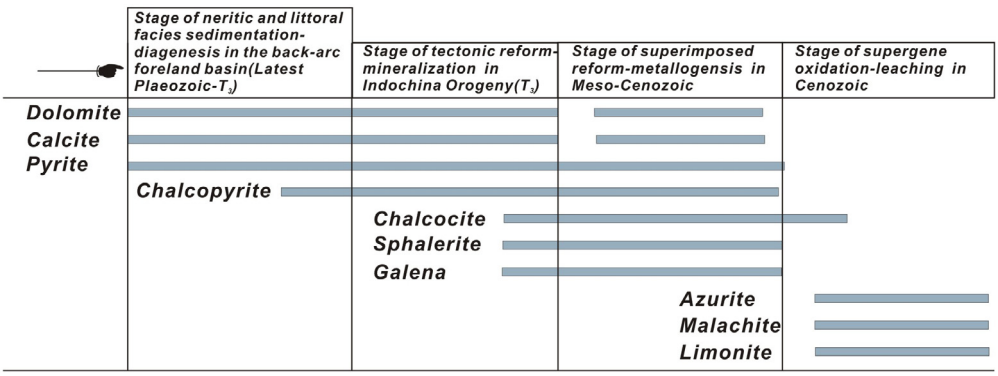

Fig. 4. Formation sequence of the major ore minerals of the BKC Cu–Pb–Ag deposit, Northern Laos.

in this geological and mineral exploration investigation to achieve better prospecting and exploration results.

Induced Polarization (IP) is an effective and a mature geophysical exploration method, playing an important role in the exploration of metallic sulfide deposits, the detection of groundwater resources, and the identification of hydrocarbon reservoirs in structural or lithologic traps (Parasnis, 1966; Ward, 1971; Cai et al., 2012; Khanikaev et al., 2012; Florsch and Muhlach, 2018). Rocks and mineralized bodies have different electrical parameters, indicating that it is possible to delineate the nature of deep ore bodies using the IP method. However, IP anomalies must be interpreted in combination with other geological, geophysical, and geochemical data (Cai et al., 2012). In addition, in areas with poor geological exploration, soil geochemical surveys should be conducted first to either quickly define the surface geochemical anomalies caused by the targeted metal minerals to narrow down the prospecting target area or obtain the nature of the ore-forming elements

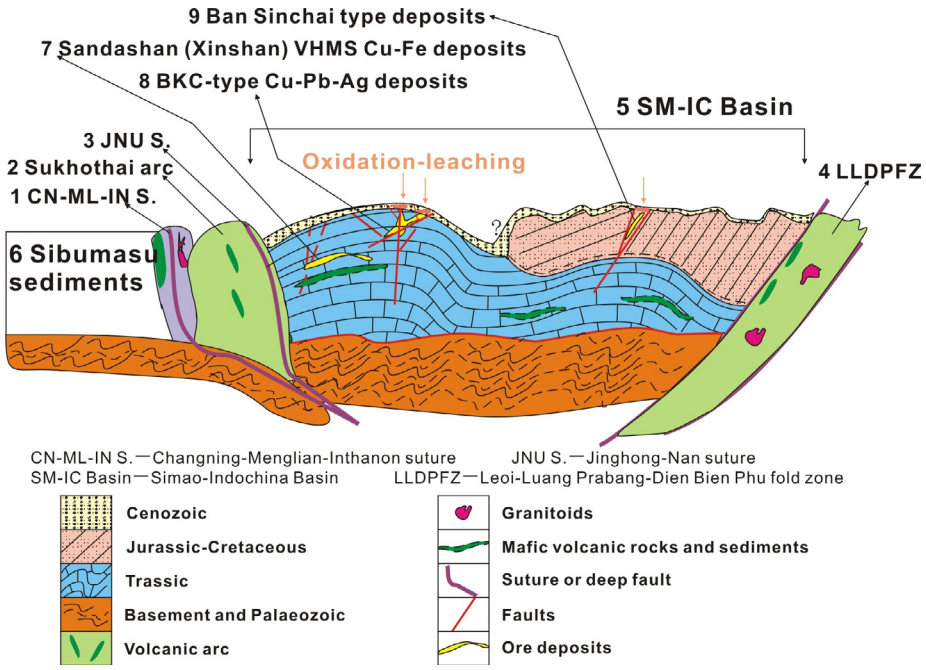

Fig. 5. A generalized mineralization model for the BKC Cu–Pb–Ag deposit and related deposits in Northern Laos: 1–(Metcalfe, 2013; Goldfarb et al., 2014; Domeier and Torsvik, 2014); 2–(Goldfarb et al., 2014; Bunopas et al., 2001); 3–(Qian et al., 2015; Hou and Zhang, 2015; Tabakh and Utha-Aroon, 1998; Fan, 2000; Yan et al., 2006); 4–(Lepvrier et al., 2004; Rossignol et al., 2016); 5–(Sone and Metcalfe, 2008; Wang et al., 2016); 6–(Thanh et al., 2011, 2014; Tabakh and Utha-Aroon, 1998; Acharyya, 1998; Otofuji et al., 2012); 7–(Khin Zaw et al., 2007; Dai et al., 2016); 8–(this study and Zhao et al., 2015); and 9–(Huang et al., 2019).

and assemblages together with other geochemical data.

Accordingly, standardized IP geophysical and soil geochemical surveys were conducted in the BKC deposit area (Fig. 6). The IP survey was powered by a WDFZ-5 high-power IP transmitter manufactured by the Chongqing Benteng Digital Control Technical Institute (CQBTSK) and was received by a CQBTSK WDJS-2 digital DC power amplifier (i.e. with the following parameters: delay = 50 ms, period = 16 s, width = 20 ms, overlay = 2 times, MN = 40 m, and dot pitch = 20 m)

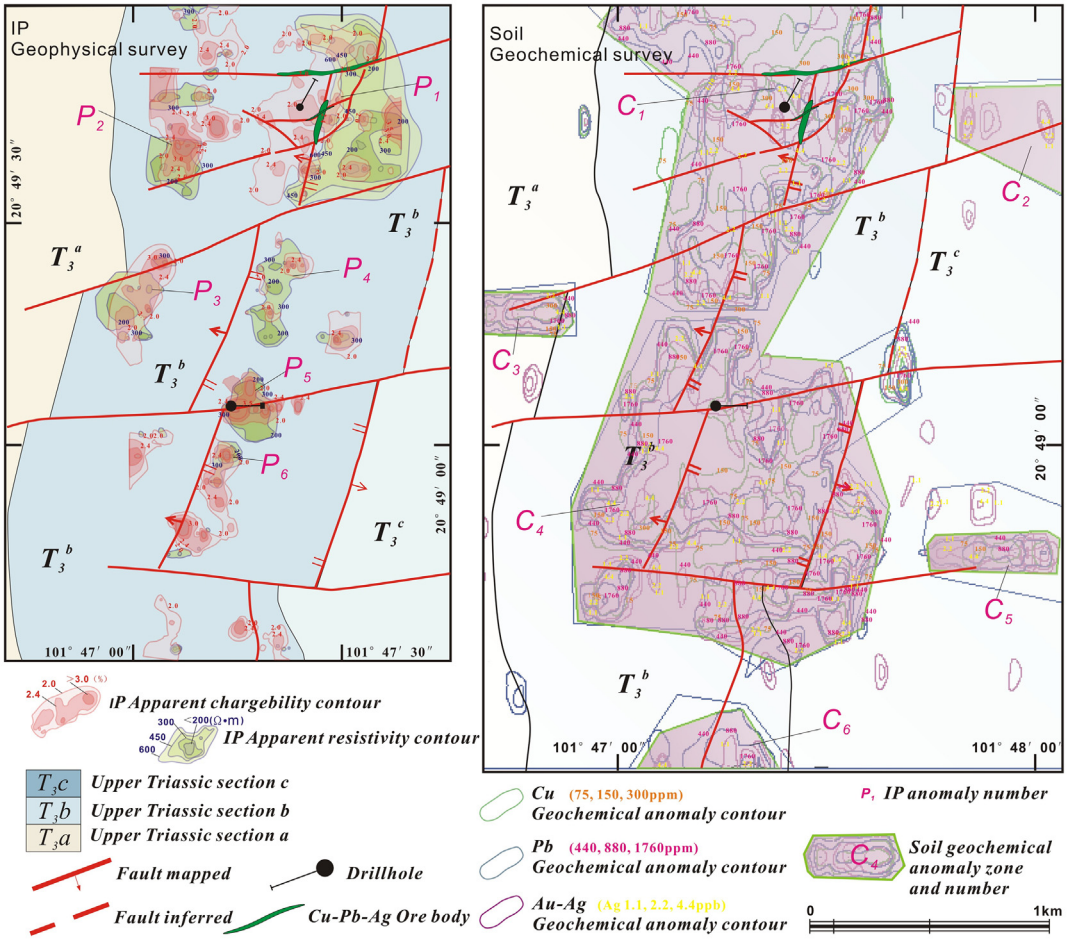

Fig. 6. Map showing the IP geophysical and soil geochemical anomalies in the BKC Cu–Pb–Ag deposit, Northern Laos.

Table 2
(A) Electrical parameters of the rock-ore samples. (B) Abnormal lower limits for the soil geochemical survey in the BKC deposit, Northern Laos.

(A) Electrical parameters of rock-ore samples

Lithology	Q(Pieces)	AR,ρs (Ω·m)		AC, ηs (%)	
		Range	Average	Range	Average
Siltstone, Sandstone	6	50–435	215	1.1–3.1	2.3
Crystalline limestone, Dolomitic Limestone	15	527–4815	672	1.0–3.1	1.4
Altered wall-rock	2	336–1225	780	2.0–3.9	3
Azurite, Galena-sphalerite	3	67–563	362	6.3–15.6	11.8

Q-Quantity; AR-Apparent Resistivity; AC-Apparent Chargeability

(B) Abnormal lower limit for the Soil geochemical survey

Elements	Lg (Co)	lg(δ)	n	lg (Ca)	calculated value (Ca)	Actual value (Ca)
Au (ppb)	−0.24	0.253	1	0.013	1.0304	1.5
Ag (ppb)	−0.791	0.687	1	−0.104	0.787	1.1
Cu (ppm)	1.586	0.335	1	1.921	83.3681	75
Pb (ppm)	1.93	0.679	1	2.609	406.4433	440

Abnormal lower limit formula: $lg(Ca) = lg(Co) + n \times lg(\delta)$; lg(Ca)-Abnormal lower limit Logarithm, lg(Co)-background content Logarithm, δ-Standard deviation, n = 1

to record the apparent polarizability (ηs), primary potential (Vp) and supply current, and equipped with an intermediate gradient device for the surface survey (i.e. with the following parameters: dot pitch AB = 1000–1400 m and power supply current I = 1000–1800 mA) and a symmetrical quadrupole sounding device (i.e. with parameters of AB/2 = 6 m, 9 m, 15 m, 25 m, 40 m, 65 m, 100 m, 150 m, 220 m, and 340 m). The working physical parameters were measured using a forced current method, and the relative error of the precision quality inspection was within the allowable range of the specification. On a 1:10,000-scaled topographic map, the IP and soil geochemical survey points were arranged according to a line–point distance network of 100 m × 20 m and 100 m × 40 m, respectively, which were determined via GPS navigation with the conversion parameters corrected by an independent coordinate system.

A total of 26 surface rock (ore) samples were collected from the survey area and their electrical parameters were determined using a forced current method (Table 2A). The elemental contents of the soil samples were obtained using the ICP-MS method, and the abnormal lower limit of each element was calculated according to the technical specifications after eliminating extremely high values and implementing the normal distribution morphology test via logarithmic grouping (Table 2B).

4.2. IP geophysical survey results

The azurite and Pb–Zn mineralized ores from the BKC deposit have a slightly high chargeability (> 11%) and a relatively low resistivity (< 500 Ω·m), which attests to their characteristics of high chargeability and low resistivity. The discrepancy between the rocks and the ores provides a good physical premise for using the IP method to sound the Cu–Pb–Zn polymetallic ore (or mineralized) body belt in the survey area. The acquired P1, P2, and P5 anomalies are characterized by high chargeability and low resistivity of mineralization anomalies, which are coincident with the mapped surface mineralization (Table 2A and Fig. 6).

The P1 anomaly area is covered with T_3b dolomitic limestone, where the rocks commonly include carbonate alteration and silicification, which are more obvious in sections that are close to faults. The fracture zones criss-cross this anomaly area where the predominant faults F_4, F_6, F_7, and F_8, also pass through (Fig. 6). Controlling and hosting the ore body I, the F_6 fault, with an occurrence of EW∠70–72°S, developed a fractured zone approximately 3-m wide, where fault breccias occur with weak silicification, strong carbonate alteration, and copper mineralization. The F_7 fault has similar fracture characteristics to those of F_6 and controls occurrence of the ore body II. Ten IP sounding profile spots (D1–D10) (Fig. 2e) were set up in the F_6 and F_7 fault distribution area to probe the existence of low resistivity and high chargeable geological bodies under the anomalies. Consequently, the IP measurement profile indicates an anomalous geological body (NGB) with high chargeability (an average ηs of 2.2%) and low resistivity (ρs < 500 Ω·m) at the depths of D2 and D8 (AB/2 > 220 m) (Fig. 7). The calculations show that the main body of the NGB should be buried deeply, at depth of approximately 100–110 m (Fig. 7) and be controlled by fracture zones. The discovery of the NGB provided a basis for further drilling verification.

4.3. Soil geochemical survey results

The soil geochemical survey provided multiple anomaly areas with high anomalous intensities, distinct concentration centers and zonation, coincident Cu–Pb–Zn–Au–Ag–As element associations, and favorable metallogenic conditions such as ore-hosting strata and ore-controlling structures (Table 3A and Fig. 6).

The C1 and C4 anomalies are likely the best anomalies (Table 3A and Fig. 6) and have a NE-trending planar and banded distribution along the T_3b strata and are large-scale with conspicuous concentration and zonation centers. The element assemblage is dominated by Cu, Pb, Zn, Ag, Sb, and As, while the Au anomalies are weak. The faults are well developed, and some parts of high Pb–Zn contents indicate the mineralization coinciding with the known surface Cu–Pb–Ag mineralization (Fig. 2e and 6). It was inferred that there is potential for a wide, continuous, and band-shaped concealed geological body in the N–S direction along the C1, C4, and C6 anomalies (Fig. 6), which was assumed to be due to hidden Cu–Pb–Zn polymetallic mineralization.

5. Ore prospecting targets and confirmation results

5.1. Ore prospecting targets

The E–W, N–S and NE–SW-trending faults are developed in locations where the IP geophysical and soil geochemical anomalies (P1-C1 and P5-C4) coincide well both with each other and with favorable stratigraphic and lithologic conditions. Meanwhile, the corresponding mineralization and ore bodies are found on the surface, nearby anomaly P1-C1 (Fig. 2e and 6). This indicates that the IP geophysical and soil geochemical surveys are applicable for exploration in this area. The discovery of highly coincident surface anomalies and IP measurement profile anomalies contributed to providing a reliable basis for further exploration verification.

Based on the geological characteristics of the BKC deposit and the IP geophysical and soil geochemical anomalies, ore exploration targets were selected (Figs. 6–8), in particular: (i) deeper extensions of the known ore bodies I and II, and; (ii) deeper parts of the overlapping anomalies (P1-C1 and P5-C4), to confirm the existence of industrial-grade mineralized bodies.

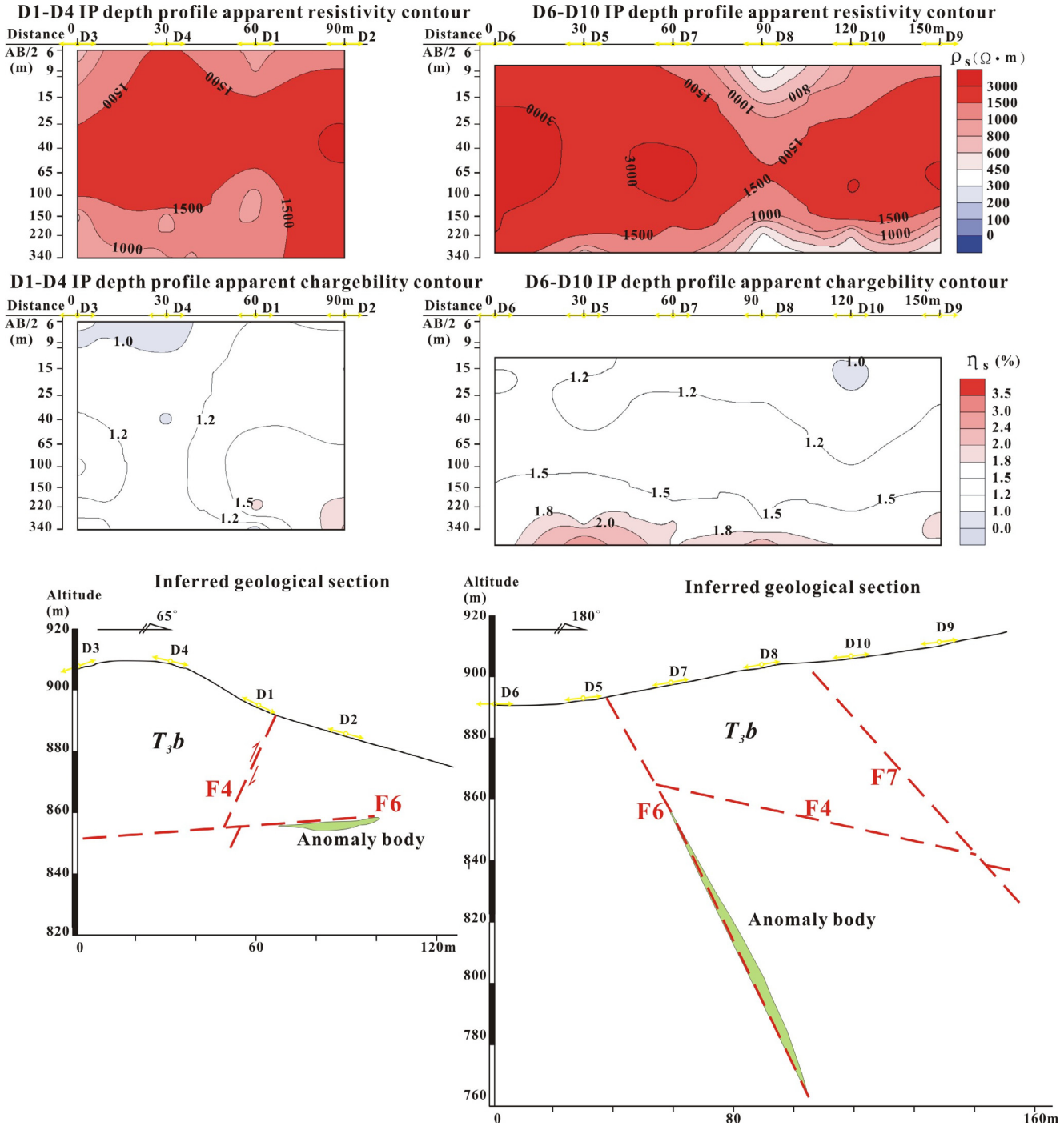

Fig. 7. IP sounding profiles showing the inferred anomalous bodies in the BKC Cu–Pb–Ag deposit, Northern Laos.

Table 3
(A) Soil geochemical anomalous values. (B) Drill hole maximum contents of the main elements at the BKC Cu–Pb–Ag deposit, Northern Laos.

Anomalous values	Cu (ppm)		Pb (ppm)		Zn (ppm)		Ag (ppm)		Au (ppb)	
Anomaly Code	Maximum	Average	Maximum	Average	Maximum	Average	Maximum	Average	Maximum	Average
C1	2018	215.14	6980	1889.6	5250	1786.4	27.5	4.86	16	9.21
C4	427	171.6	5975	1737.8	10,000	2482	15	5.49	5.2	2.29
(B)Max-content	Cu (%)		Pb (%)		Zn (%)		Ag (g/t)		Au (g/t)	
ZK001	0.024		0.21		0.32		6.5		0.02	
ZK2301	0.068		0.062		0.086		1.6		0.18	

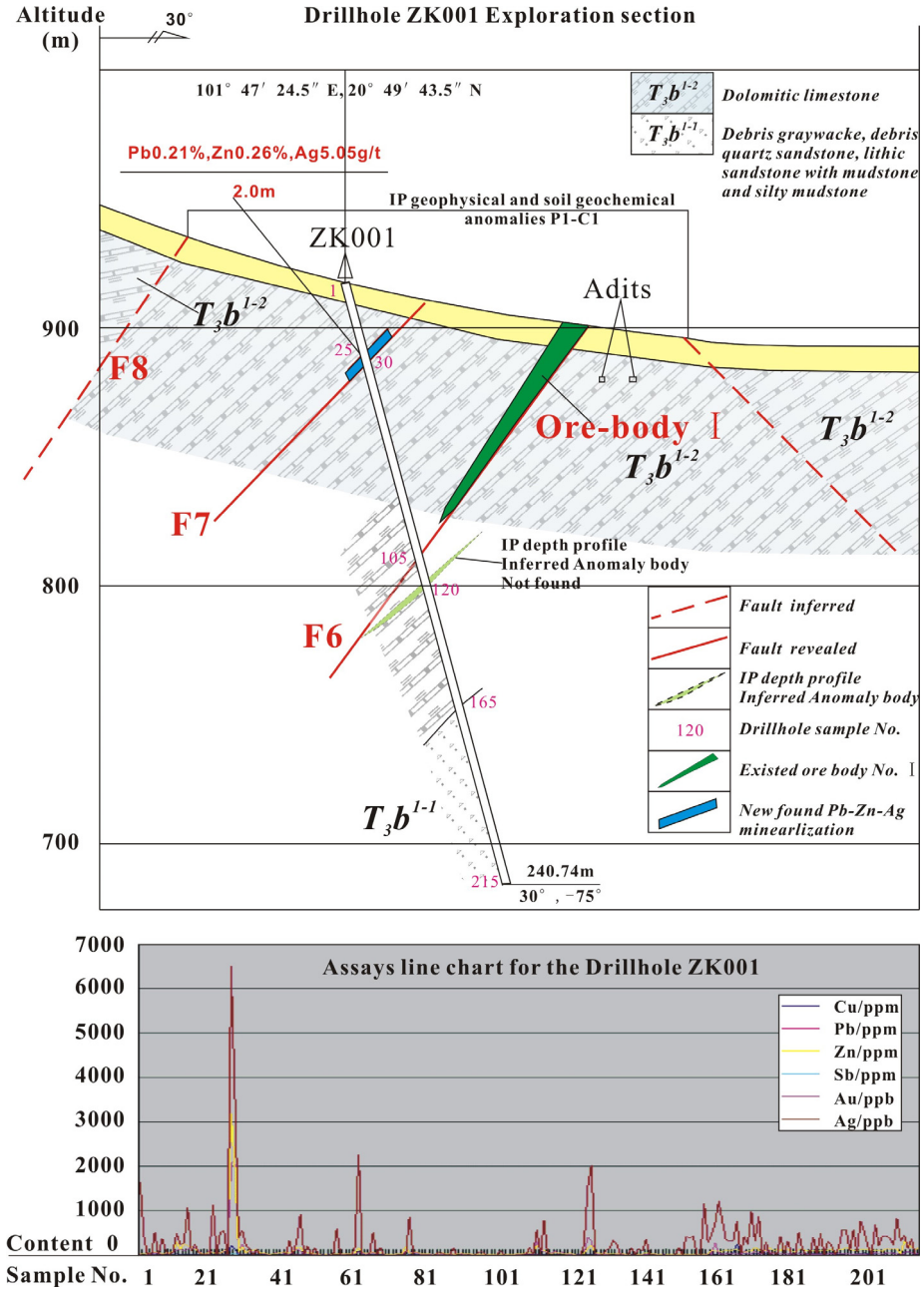

Fig. 8. Prospecting profile of the drill hole ZK001 verifying the anomalies, showing the revealed Pb–Zn–Ag mineralization in the BKC Cu–Pb–Ag deposit, Northern Laos.

5.2. Prospect confirmation results

By screening the IP geophysical and soil geochemical anomalies, two anomalies P1-C1 and P5-C4, which are well matched with the available geological and metallogenic conditions, both appear to be obvious targets for surface trenching and drilling confirmation. A mineralized outcrop of 23 m × 2 m in size was exposed on the surface trench of the ore body I with grades of 0.92% Cu and 54.8 g/t Ag, and an 8 m × 1 m-sized outcrop was exposed on the surface trench of the ore body II with grades of 3.06% Cu and 99.1 g/t Ag (Fig. 2e). Two completed drill holes, namely: ZK001 (030° collared azimuth, −75° inclination and 240.74 m depth) and ZK2301 (090° azimuth, −75°inclination and 318.25 m depth), tested the P1-C1 and P5-C4 anomaly areas below surface (Fig. 2e and 8). Unexpectedly, the two drill holes revealed no corresponding ore bodies, except for a 2-m-thick Pb–Zn–Ag mineralized zone in the F_7 fault belt at a depth of 26–28 m by drill hole ZK001 (Fig. 8). Meanwhile, the maximum contents of the target elements failed to reach minable grades (Table 3B). The interpreted anomalous body at the depth of 100–110 m, given by the IP depth measurement profile (Fig. 7), was shown to be equivalent to the F_6 fault zone, as intersected by drill hole ZK001. This indicates that the ore body I, controlled by F_6, does not extend downward along the fault zone but is only a small-scale ore body at shallow depth (Fig. 8). By drilling confirmation, the IP geophysical and soil geochemical anomalies only existed on the surface of the T_3b dolomitic limestone areas and the faulted areas (Fig. 6), rather than corresponding to the ore-induced anomalies. This result is inconsistent with the characteristics of large-scale, well-matched, concentrated and zoning elements and good-potential-indicated anomalies. Therefore, these observations are advocating that the geophysical and geochemical anomalies should be distinguished carefully together with the other data, prior to further exploration and engineering investments being undertaken.

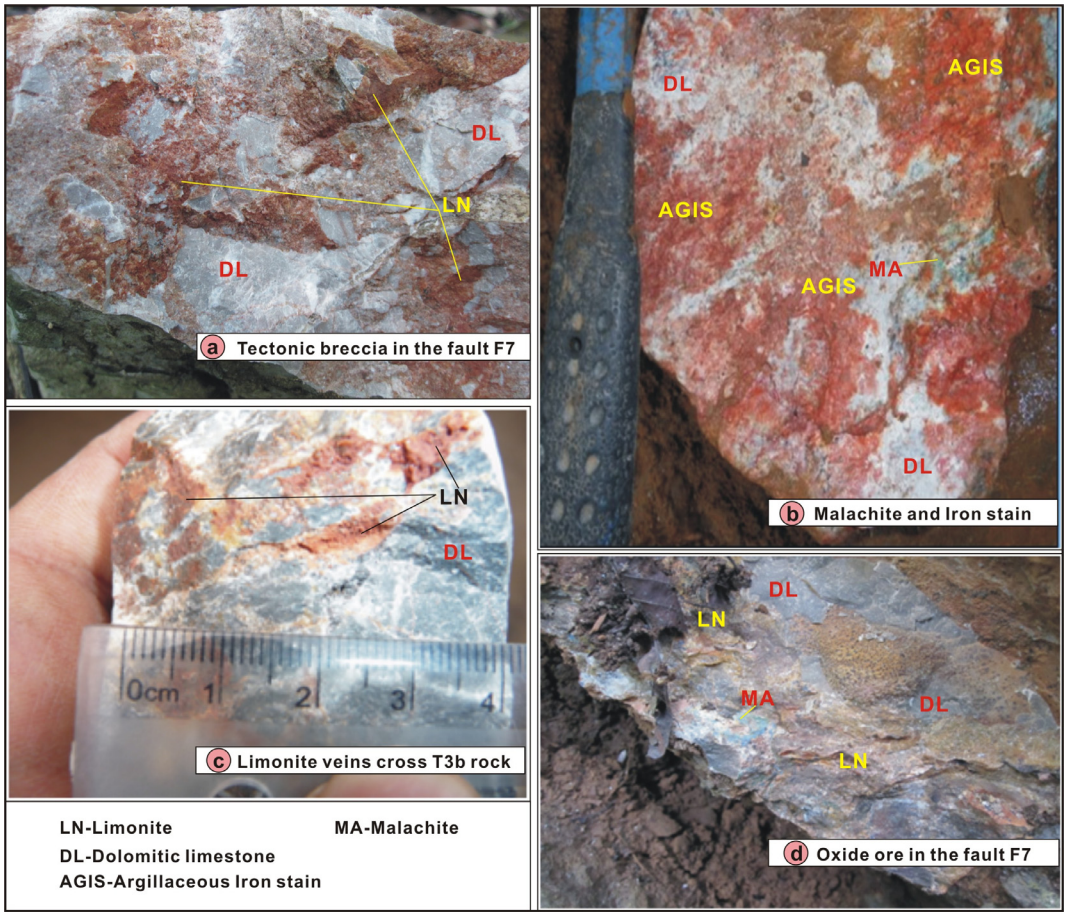

Fig. 9. Rock fabric pictures, showing the leached ferrous veins in the BKC Cu–Pb–Ag deposit, Northern Laos.

A new understanding is therefore required of the ore-forming conditions of the BKC Cu–Pb–Ag deposit area. In particular, this area has a relatively monotonous stratigraphic lithology and is moderately folded without obvious magmatic activities, and most of the faults are post-mineralization deformed structures. The ZK001 drill core intersected fracture zones and 1–3 mm sized pyrite cubes with red iron-stained leached limestone in the upper fragmented part of the core, which indicates the existence of hydrothermal activity. The revealed Pb–Zn–Ag mineralization, controlled by the interlayer fault zones, appears to have formed by medium–low-temperature hydrothermal fluid, which supposedly implies the presence of hydrothermal (Cu–Pb–Zn–Ag–Au) activities along the regional fracture zones (Fig. 5). It further indicates that the genetic relationships and hydrothermal processes between the formation of the BKC deposit and the regional setting needs to be investigated and that mineral prospecting should be aimed at structures and formations embedded within the volcanic–magmatic rocks, which may lead to the discovery of other deposit types (e.g., VHMS and skarn types related to volcanic–magmatic activity) in the SM-IC Basin (Fig. 5).

6. Discussions

6.1. Mineralization features of the BKC deposit

The following tectonic setting and the nature and criteria of the mineralization are important.

(1) The relatively high background values of ore-forming elements such as Cu, Fe, Pb, Zn, and Ag in the T_3b formation: The Triassic neritic facies sedimentation with volcanic-sedimentary activities in the continental margin existed in the BKC deposit and even in the SM-IC Basin, where some VHMS Cu–Fe–Pb–Zn polymetallic deposits occurred (e.g., Khin Zaw et al., 2007; Dai et al., 2016). This may imply that the area has an abundant ore-forming element synchronously enriched in the strata with high background values of Cu–Fe–Pb–Zn. In addition, this may provide a conceptual basis for the presence of large-scale geophysical and geochemical anomalies along the T_3b Formation and the fault zones therein.

(2) Structural setup through interconnected fractures with each other in the area: The Indosinian Orogeny and Mesozoic–Cenozoic regional tectonic movements yielded intense tectonic deformation and volcanic–magmatic activities throughout Northern Laos (Fig. 1), which simultaneously resulted in an earlier stage of relatively large-scale N–S-trending folds and faults, NW -trending secondary folds and faults, and later stage of E-W-trending faults (such as F_6 and F_7) and NE-trending faults in the BKC deposit area (Figs. 1 and 2). These structures cut through and interconnected with each other, forming fluid migration channels that penetrated and reformed the existing structures and strata.

A number of fracture zones pass through the area of the anomaly sections (Fig. 2). The occurrence of the strata and rocks in the BKC deposit area was controlled by the large-scale nearly N–S-trending F_1 fault that had likely connected with regional tectono–magmatic hydrothermal activities (Fig. 2d). Each of the nearly E-W-trending F_6 and F_7 faults control the occurrence of the ore bodies I and II respectively, have a fracture zone that is approximately 3-m wide, with fault breccias, weak silicification, strong carbonatization (calcite and dolomite veins and masses), and Cu mineralization, such as malachite, azurite, and a little chalcocite and chalcopyrite. Other faults also commonly have 1–2-m-wide fracture zones and breccias. The joints and fissures are well developed in the rocks near the faults with stockwork silicification, carbonate alteration, and limonitization distributed along the

fissures.

(3) Strong hydrothermal activities: During the regional tectonic–hydrothermal events, Fe, Cu, Pb, Zn, Ag, and Au elements were leached from the regional strata by hydrothermal fluids, and then migrated along the N–S-trending faults to deposit in the nearly E-W-trending fault zones and in con-junctions with other faults. Meanwhile, the rocks near the fracture zones generally underwent carbonate alteration, silicification and other alterations (Fig. 3). For example, the ZnO contents in altered dolomite and dolomitic limestone varies from 0.01% to 0.04% and are even > 0.2% in some samples, while the contents of PbO change from 0.01% to 0.17%.

(4) Widespread oxidation–leaching and lateritization: Altered rocks, mineralized bodies, and tectonic zones are usually broken up and porous which facilitated the scope and depth of the weathering and oxidation–leaching process, especially near the surface and shallow underground areas. Accordingly, the rock fissures are usually filled with reddish–brown and yellow–brown argillaceous iron stains (iron oxides) (Fig. 9), which is featured by relatively high contents of Fe–Pb–Zn–Ag (–Cu) and locally distributed azurite–malachite veinlets (e.g., trench TC18). Through the tectonic activities, they were all subjected to long-term oxidation–leaching, weathering–denudation, and lateritization, eventually forming Cu–Pb–Zn–Ag–Fe-bearing laterites. The shallow parts of the primary-mineralization zones were translated into oxidized ore bodies and mineralized outcrops, predominated by azurite–malachite–limonite along the fracture zones (Fig. 2e; Fig. 3). For example, a black–brown polymetallic zone (i.e. with 0.014% Cu, 7.8% Pb, 0.27% Zn, and 3.9 g/t Ag), approximately 40-m long and 50-m wide, was found in the overburden of the trench TC16 and also within the planar geophysical–geochemical anomalies P5-C4. This zone is at a distance of approximately 200 m to the east of the subsequent drill hole ZK2301 in the middle of the BKC deposit area (Fig. 2b; Fig. 7).

The laterite samples from the anomalous areas have contents of 0.29–0.69% Pb, 0.41–1% Zn, ~0.2% Cu, and 3–43 g/t Ag (i.e. soil samples D032–D35), which indicate that low-grade laterite Ag mineralized bodies can be delineated in some areas. The characteristics of the Cu–Pb–Zn–Ag ore bodies hosted in carbonate rocks and the weathered laterite Ag mineralization can be compared to those of the Lancang Pb–Zn deposit (Fan, 1985; Chen, 2002) and the Lancang laterite Ag deposit (Chen et al., 2000; Chen et al., 2002) in Yunnan Province of SW China, as well as the laterite Au deposits in Northern Laos (Hu et al., 2013; Wang and Shi, 2016).

6.2. Causes of the geophysical anomalies

On the basis of the regional geological setting and the mineralization features noted above, we provide interpretation on the main causes of the IP geophysical anomalies: (i) faults, fissures, and fractured zones were well developed and active in the area, resulting in fragmented rocks and enabling large-scale metal-rich hydrothermal activities to form rock alteration and localized mineralization (Fig. 2), and (ii) later stage oxidation leaching and lateritization promoted in-situ dispersion and local supergene enrichment of Fe–Cu–Pb–Zn–Ag elements, presenting the high polarizability and low resistivity differences that caused band-shaped anomalies to be widely distributed along the T_3b formation and fault zones therein (Fig. 6).

6.3. Causes of the geochemical anomalies

Similarly, the main causes of the soil geochemical anomalies are likely: (i) the ore-forming elements such as Cu–Fe–Pb–Zn (–Ag) in the T_3b formation which have high content background values, (ii) different trending faults cross-cut and interconnected with each other (Fig. 2), forming fluid migration pathways linking the regional tectono–magmatic–hydrothermal activities (Khin Zaw et al., 2014; Kamvong et al., 2014; Goldfarb et al., 2014). This created strong water–rock interactions in the forms of silicification and carbonization alteration, and the Cu–Fe–Pb–Zn (–Ag) mineralization along the fissures, and (iii) the dispersion and secondary enrichment of these elements on the surface laterite (soil) contributed to produce superficial anomalies throughout the area (Fig. 6).

6.4. Implications and significance for regional mineral prospecting

The Paleozoic western margin of the SM-ICB was positioned in a back-arc basin and island arc tectonic setting (Metcalfe, 2002, 2013; Lepvrier et al., 2004; Yan et al., 2006; Sone and Metcalfe, 2008; Qian et al., 2015; Wang et al., 2016; Merdith et al., 2017). Along with the closure of the Paleo-Tethys Ocean from late Paleozoic to late Triassic (Sone and Metcalfe, 2008), the SM-IC Basin was formed to deposit the Triassic neritic facies carbonate rocks intercalated with volcanic-related pyroclastic sedimentary rocks (Golonka, 2007; Deng and Wang, 2016; Li et al., 2018; Khin Zaw et al., 2014). The sequences are rich in Cu, Au, Ag, Pb, and Zn elements. In the late Triassic, the exhumation of the Paleozoic JNU back-arc basin (Metcalfe, 2002, 2013; Lepvrier et al., 2004; Yan et al., 2006; Sone and Metcalfe, 2008; Faure et al., 2017; Qian et al., 2015; Hou and Zhang, 2015) and the folding and deformation of the L-L-BBPFB (Bunopas et al., 2001; Goldfarb et al., 2014) were accompanied by volcanic–magmatic intrusions (Lepvrier et al., 2004), which transported numerous ore-forming elements up from depth. During the Mesozoic and Cenozoic, the SM-IC Basin was subjected to denudation and sedimentation from both the east and the west sides, and multi-stage regional tectono–magmatic activities were superimposed upon the earlier volcanic sedimentary sequences (Zhang et al., 1999; Acharyya, 2000; Wang et al., 2001; Morley, 2002; Yin, 2010). This event initiated the formation of VHMS, SEDEX, skarn, volcanic–sedimentary, hydrothermal types of Cu, Au, Fe, Pb, Zn deposits and epithermal, sediment-hosted/orogenic types of Au deposits, as well as gemstone deposits in Northern Laos. They were related to the continental sedimentation, tectonic movements, volcanic activities and magmatic intrusions in the SM-IC Basin and its surrounding areas (Table 1). Important deposit examples are the Jinding super-large stratabound Zn–Pb–Ag deposit (Khin Zaw et al., 2007) and the Jinman sandstone-type Cu deposit, the Guanfang VHMS Cu deposit, the Dapingzhang VHMS (or SEDEX) Cu–Zn polymetallic deposit (Dai et al., 2004; Khin Zaw et al., 2007), the Sandashan Triassic-cupriferous Cu deposit (Khin Zaw et al., 2007), the Xinshan volcano–sedimentary Fe–Cu deposit and the sandstone-type deposits of Nanpo, Yaojiashan, and Ban Sinchai (Huang et al., 2019), the Ban Namor and Phu Thung Late-Triassic Cu deposits (Zhao et al., 2015), the Lancang Laochang Pb–Zn deposit (Fan, 1985; Chen et al., 2002) and laterite Ag deposit (Chen et al., 2000, 2002), and the Phapon and Pankham laterite Au deposits in Northern Laos (Hu et al., 2013; Wang and Shi, 2016).

As a representative hydrothermal Cu polymetallic deposit in Northern Laos, the BKC Cu–Pb–Ag deposit is controlled by fault zones cutting through the Triassic dolomitic limestone formation and is inextricably linked with important types of ore mineralization and deposits above (Table 1). The prospecting of the BKC deposit provides a case study and prompt example for the exploration of other related deposits in the metallogenic system of the SM-IC Basin. Our prospecting experience and this research results can be expanded as effective reference and prospecting potential as well as to study the genesis of the related deposits.

As a result, it is suggested that the typical strata of the Paleozoic back-arc and island-arc environment in/or around the SM-IC Basin should be incorporated when we plan for prospecting and exploration for ore deposits such as: (i) Triassic Fe, Cu, Pb–Zn, and Ag–Au polymetallic deposits related to volcanic activities, and (ii) hydrothermal Cu–Pb–Ag polymetallic deposits related to regional tectonics or intermediate–flesic magmatic activities, as well as (iii) laterite Ag (Au) deposits.

7. Conclusions

(1) The BKC Cu–Pb–Ag deposit is structurally controlled by fault zones and is hosted by the upper Triassic carbonate rocks in the Mesozoic–Cenozoic red bed SM-IC Basin of Northern Laos. It is noteworthy that the discovery of laterite Ag mineralization is recorded in the BKC deposit area.
(2) Large-scale and highly overlapping comprehensive anomalies were identified in the BKC deposit by using IP geophysical and soil geochemical surveys. The extension areas of the known ore bodies I and II with the two anomalies P1-C1 and P5-C4, were selected for further verification of target areas by exploration drilling. However, no expected Cu ore bodies, except for a 2-m-wide Pb–Zn mineralized zone, were found by the two drill holes testing the P1-C1 and P5-C4 anomalies.
(3) The BSK anomalies were primarily generated by the in-situ dispersion and secondary supergene enrichment of ore-forming elements such as Fe, Cu, Pb, and Zn (Ag), which may be due to their pre-existing high background values in the hosting strata, along with strong fault-dissections and hydrothermal alterations, and then intense oxidation leaching and lateritization in the later stage.
(4) The study on the geological, geochemical and geophysical characteristics of the BKC deposit and the subsequent prospecting lessons learnt, suggest that there remains the potential for discovery of the other related VHMS, SEDEX, skarn, hydrothermal Cu polymetallic deposits and epithermal, sediment-hosted/orogenic Au deposits, as well as the laterite Ag (Au) deposits in the SM-IC Basin of Northern Laos.

Declaration of Competing Interest

The authors declare that they have no known competing financial interests or personal relationships that could have appeared to influence the work reported in this paper.

Acknowledgments

This study is funded by the National 973 Program of China (2014CB440906). We thank Yunnan Copper Industry (Group) Co., Ltd. for its support of this research. We thank the reviewers, the editors, and Profs. Ruizhong Hu, Zhilong Huang, and Xianwu Bi (Institute of Geochemistry, CAS) and Prof. Jiaxi Zhou (Yunnan University) for the valuable suggestions. We appreciate Prof. Xiaoyong Yang's recommendation. The first author also thank Mr. Achong Laomao (Director of Investment Department, Ministry of Planning and Investment, Lao PDR), Dr. Khampha Phommakaysone (Director of Geology Department, Ministry of Natural Resources and Environment, Lao PDR) and Simon Pijid (Director of Mining Department, Ministry of Energy and Mines, Lao PDR) for the help. Paul Cromie and Khin Zaw are thankful to previous and current colleagues from CODES, University of Tasmania for their constructive discussion and comments.

References

Acharyya, S.K., 1998. Break-up of the Greater Indo-Australian Continent and accretion of blocks framing South and East Asia. J. Geodyn. 26 (1), 149–170.
Acharyya, S.K., 2000. Break Up of Australia-India-Madagascar Block, Opening of the Indian Ocean and Continental Accretion in Southeast Asia With Special Reference to the Characteristics of the Peri-Indian Collision Zones. Gondwana Res. 3 (4), 425–443.
Bui, H.B., Ngo, X.T., Khuong, T.H., Golonka, J., Nguyen, T.D., Song, Y., Itaya, T., Yagi, K., 2017. Episodes of brittle deformation within the Dien Bien Phu Fault zone, Vietnam: Evidence from K-Ar age dating of authigenic illite. Tectonophysics 695, 53–63.
Bunopas, S., Vella, P., Fontaine, H., Hada, S., Burret, C., Haines, P., Potisat, S., Wongwanich, Th., Chaodamrong, P., Howard, K.T., Khositanont, S., 2001. Growth of Asia in the Late Triassic Continent-Continent Collision of Shan-Thai and Indochina Against South China. Gondwana Res. 4 (4), 584–585.
Cai, Y.S., Yin, H.Y., Zhang, J.G., Xia, X.Y., 2012. Discussion on working principle and application effect of polarization method. Mineral Exploration 3 (2), 212–218 (In Chinese with English abstract).
Chen, B.Y., 2002. Study on metallogeny of the Laochang Ag-Pb-Zn-Cu polymetallic ore deposit of Lancang, Yunnan[D]. Central South University, 1-115 (In Chinese with English Abstract).
Chen, B.Y., Wang, Z.R., Zhang, Y.X., Chen, W., 2000. Metallogenic conditions and prospecting criteria of Laochang lateritic silver deposit, Lancang. Journal of Central Souh University of Technology 31(3), 195-198 (In Chinese with English Abstract).
Chen, B.Y., Wang, Z.R., Peng, S.L., Zhang, Y.X., Chen, W., 2002. Geology and Genesis of the Lateritic type Ag-Mn ore deposit at Laochang, Lancang area. Geotectonic et Metallogenia 26 (1), 86–91 (In Chinese with English Abstract).
Cheng, X., Shen, L., Gao, T.M., 2011. Development Status of Mineral Resources in Five Countries of the Indochina Peninsula and Investment Preferences for China. Resources Science 33 (10), 1847–1854 (in Chinese with English abstract).
Cromie, P., 2010. Geological setting, geochemistry and genesis of the Sepon gold and copper deposits, Laos. Unpublished PhD thesis, ARC Centre of Excellence in Ore Deposits (CODES), University of Tasmania, Hobart, Austalia, p. 395.
Cromie, P., Makoundi, C., Khin Zaw, Cooke, D.R., White, N., Ryan, C., 2018. Geochemistry of Au-bearing pyrite from the Sepon Mineral District, Laos DPR, Southeast Asia: Implications for ore genesis. Journal of Asian Earth Sciences 164, 194-218.
Dai, B.Z., Liao, Q.L., Jiang, S.Y., 2004 Isotope Geochemistry and Mineralization Age of the Dapingzhang Copper-polymetallic Deposit in Lanping-Simao Basin, Yunnan Province. Journal of Nanjing University (Natural Sciences) 40(6), 674-683 (In Chinese with English Abstract).
Dai, P.Y., Wang, D.K., Xie, F.Y., 2016. The geologic feature and prospecting criteria of Xinshan Fe deposit in Mengla. Yunnan. Yunnan Geology 35 (1), 9–14 (In Chinese with English abstract).
Deng, J., Wang, Q.F., Li, G.J., Zhao, Y., 2015. Structural control and genesis of the Oligocene Zhenyuan orogenic gold deposit, SW China. Ore Geol. Rev. 65, 42–54.
Deng, J., Wang, Q.F., 2016. Gold mineralization in China: Metallogenic provinces, deposit types and tectonic framework. Gondwana Res. 36, 219–274.
Dill, H.G., Weber, B., 2013. Gemstones and geosciences in space and time digital maps to the "Chessboard classification scheme of mineral deposits. Earth Sci. Rev. 127, 262–299.
Domeier, M., Torsvik, T.H., 2014. Plate tectonics in the late Paleozoic. Geosci. Front. 5, 303–350.
Fan, C.J., 1985. Discussion on the origin and the regional geological background of Laochang Pb-Zn deposits in Lancang county. Yunnan Geology 4 (1), 1–6.
Fan, P.F., 2000. Accreted terranes and mineral deposits of Indochina. J. Asian Earth Sci. 18, 343–350.
Fan, W.M., Wang, Y.J., Zhang, A.M., Zhang, F.F., Zhang, Y.Z., 2010. Permian arc-back-arc basin development along the Ailaoshan tectonic zone: Geochemical, isotopic and geochronological evidence from the Mojiang volcanic rocks, Southwest China. Lithos 119, 553–568.
Faure, M., Lepvrier, C., Nguyen, V.V., Vu, T.V., Lin, W., Chen, Z.C., 2014. The South China block-Indochina collision: Where, when, and how? J. Asian Earth Sci. 79, 260–274.
Faure, M., Chen, Y., Feng, Z.H., Shu, L.S., Xu, Z.Q., 2017. Tectonics and geodynamics of South China: An introductory note. J. Asian Earth Sci. 141, 1–6.
Feng, Q.L., Chonglakmani, C., Helmcke, D., Ingavat-Helmcke, R., Liu, B.P., 2005. Correlation of Triassic stratigraphy between the Simao and Lampang-Phrae Basins: implications for the tectonopaleogeography of Southeast Asia. J. Asian Earth Sci. 24, 777–785.
Ferrari, O.M., Hochard, C., Stampfli, G.M., 2008. An alternative plate tectonic model for the Palaeozoic-Early Mesozoic Palaeotethyan evolution of Southeast Asia (Northern Thailand–Burma). Tectonophysics 451, 346–365.
Florsch, N., Muhlach, F., 2018. 4 - The Induced Polarization (IP) Method. Everyday Applied Geophysics 1, Elsevier, 121-133. (https://doi.org/10.1016/B978-1-78548-199-4.50004-0).
Gao, Y.L., Niu, Y.J., Liu, Z.Y., Chen, J.Y., Shen, J.Z., 2017. Gold Resources Distribution Characteristics and Metallogenic Potential of Laos. Modern Mining 5 (5), 20–25 (in Chinese with English abstract).
Goldfarb, R.J., Taylor, R.D., Collins, G.S., Goryachev, N.A., Orlandini, O.F., 2014. Phanerozoic continental growth and gold metallogeny of Asia. Gondwana Res. 25, 48–102.
Golonka, J., 2007. Late Triassic and Early Jurassic palaeogeography of the world. Palaeogeogr. Palaeoclimatol. Palaeoecol. 244, 297–307.
Hou, Z.Q., Zhang, H.R., 2015. Geodynamics and metallogeny of the eastern Tethyan metallogenic domain. Ore Geol. Rev. 70, 346–384.
Huang, J.G., Ren, T., Zou, H.J., 2019. Genesis of Xinzhai Sandstone-Type copper deposit in Northern Laos: Geological and Geochemical Evidences. J. Earth Sci. 30 (1), 95–108.
Huang, K.N., Opdyke, N.D., 2016. Paleomagnetism of the Upper Triassic rocks from south of the Ailaoshan Suture and the timing of the amalgamation between the South China and the Indochina Blocks. J. Asian Earth Sci. 119, 118–127.
Hu, J.C., Zhi, D.Q., Zhu, Y.P., 2013. The geological characteristics and ore genesis of laterite gold mineralization in Laos Phapon. Contributions to Geology and Mineral Resources Research 28 (3), 462–467 (In Chinese with English abstract).
Jia, R.X., Fang, W.X., Wei, X.Y., 2014. General introduction of geology, mineral resources and mining exploitation in Laos. Mineral Exploration 5 (5), 826–833 (in Chinese with English abstract).
Kamvong, T., Zaw, Khin, 2009. The origin and evolution of skarn-forming fluids from the Phu Lon deposit, northern Loei Fold Belt, Thailand: Evidence from fluid inclusion and sulfur isotope studies. J. Asian Earth Sci. 34, 624–633.
Kamvong, T., Zaw, Khin, Meffre, S., Maas, R., Stein, H., Lai, C.K., 2014. Adakites in the Truong Son and Loei fold belts, Thailand and Laos: Genesis and implications for geodynamics and metallogeny. Gondwana Res. 26, 165–184.

Khanikaev, A. B., Mousavi, S. H. , Wu, C., Dabidian, N., Alici, K.B., Shvets, G., 2012. Electromagnetically induced polarization conversion. Optics Communications 285, 3423–3427.(https://doi.org/10.1016/j.optcom.2012.03.023).
Zaw, Khin, Peters, S.G., Cromie, P., Burrett, C., Hou, Z.Q., 2007. Nature, diversity of deposit types and metallogenic relations of South China. Ore Geol. Rev. 31, 3–47.
Zaw, Khin, Meffre, S., Lai, C.K., Burrett, C., Santosh, M., Graham, I., Manaka, T., Salam, A., Kamvong, T., Cromie, P., 2014. Tectonics and metallogeny of mainland Southeast Asia — A review and contribution. Gondwana Research 26, 5–30.Lai, K.Y., Chen, Y.G.u, Lâm, D.Đ., 2012. Pliocene-to-present morphotectonics of the Dien Bien Phu fault in northwest Vietnam. Geomorphology 173–174, 52–68.
Lepvrier, C., Maluski, H., Tich, V.V., Leyreloup, A., Thi, P.T., Vuong, N.V., 2004. The Early Triassic Indosinian orogeny in Vietnam (Truong Son Belt and Kontum Massif): implications for the geodynamic evolution of Indochina. Tectonophysics 393, 87–118.
Li, S.Z., Zhao, S.J., Liu, X., Cao, H.H., Yu, S., Li, X.Y., Somerville, I., Yu, S.Y., Suo, Y.H., 2018. Closure of the Proto-Tethys Ocean and Early Paleozoic amalgamation of microcontinental blocks in East Asia. Earth Sci. Rev. 186, 37–75.
Liu, H.C., Wang, Y.J., Cawood, P.A., Fan, W.M., Cai, Y.F., Xing, X.W., 2015. Record of Tethyan ocean closure and Indosinian collision along the Ailaoshan suture zone (SW China). Gondwana Res. 27, 1292–1306.
Liu, H.C., Wang, Y.J., Zi, J.W., 2017. Petrogenesis of the Dalongkai ultramafic-mafic intrusion and its tectonic implication for the Paleotethyan evolution along the Ailaoshan tectonic zone (SW China). J. Asian Earth Sci. 141, 112–124.
Makoundi, C., Zaw, Khin, Large, R.R., Meffre, S., Lai, C.K., Hoe, T.G., 2014. Geology, geochemistry and metallogenesis of the Selinsing gold deposit in Central Malaysia. Gondwana Res. https://doi.org/10.1016/j.gr.2013.08.023.
Manaka, T., Zaw, Khin, Meffre, S., Vasconcelos, P.M., Golding, S.D., 2014. The Ban Houayxai epithermal Au-Ag deposit in the Northern Lao PDR: Mineralization related to the Early Permian arc magmatism of the Truong Son Fold Belt. Gondwana Res. 26, 185–197.
Manini, A.J., Aquino, J., Gregory, C., Aneka, S., 2001. Discovery of the Sepon district gold and copper deposits. NewgGenGold, Laos, pp. 93–108.
Merdith, A.S., Collins, A.S., Williams, S.E., Pisarevsky, S., Foden, J.D., Archibald, D.B., Blades, M.L., Alessio, B.L., Armistead, S., Plavsa, D., Chris, Clark, Müller, R.D., 2017. A full-plate global reconstruction of the Neoproterozoic. Gondwana Res. 50, 84–134.
Metcalfe, I., 2002. Permian tectonic framework and palaeogeography of SE Asia. J. Asian Earth Sci. 20, 551–566.
Metcalfe, I., 2013. Gondwana dispersion and Asian accretion: Tectonic and palaeogeographic evolution of eastern Tethys. J. Asian Earth Sci. 66, 1–33.
Middlemost, E.A.K., 1972. A simple classification of volcanic rocks. Bull. Volcanol. 36, 382–397.
Morley, C.K., 2002. A tectonic model for the Tertiary evolution of strike–slip faults and rift basins in SE Asia. Tectonophysics 347, 189–215.
Otofuji, Y., Tung, V.D., Fujihar, M., Tanaka, M., Yokoyama, M., Kitada, K., Zaman, H., 2012. Tectonic deformation of the southeastern tip of the Indochina Peninsula during its southward displacement in the Cenozoic time. Gondwana Res. 22, 615–627.
Parasnis, D.S., 1966. Chapter 7 - Induced Polarization Methods. Methods in Geochemistry and Geophysics, Elsevier 3, 187-207. (https://doi.org/10.1016/B978-1-4832-3030-6.50013-4).
Qian, X., Feng, Q.L., Yang, W.Q., Wang, Y.J., Chonglakmani, C., Monjai, D., 2015. Arc-like volcanic rocks in NW Laos: Geochronological and geochemical constraints and their tectonic implications. J. Asian Earth Sci. 98, 342–357.
Qian, X., Wang, Y.J., Feng, Q.L., Zi, J.W., Zhang, Y.Z., Chonglakmani, C., 2016. Petrogenesis and tectonic implication of the Late Triassic post-collisional volcanic rocks in Chiang Khong, NW Thailand. Lithos 248–251, 418–431.
Roger, F., Jolivet, M., Maluski, H., Respaut, J.P., Münch, P., Paquette, J.L., Van, T.V., Van, V.N., 2014. Emplacement and cooling of the Dien Bien Phu granitic complex: Implications for the tectonic evolution of the Dien Bien Phu Fault (Truong Son Belt, NW Vietnam). Gondwana Res. 26, 785–801.
Rossignol, C., Bourquin, S., Poujol, M., Hallo, E.t, Dabard, M.P., Nalpas, T., 2016. The volcaniclastic series from the Luang Prabang Basin, Laos: A witness of a Triassic magmatic arc? Journal of Asian Earth Sciences 120, 159-183.
Salam, A., Zaw, Khin, Meffre, S., McPhie, J., Lai, C.K., 2014. Geochemistry and geochronology of the Chatree epithermal gold-silver deposit: Implications for the tectonic setting of the Loei Fold Belt, central Thailand. Gondwana Res. 26, 198–217.
Sangsomphong, A., Thitimakorn, T., Charusiri, P., 2015. Interpretation of tectonic setting in the Phetchabun Volcanic Terrane, Northern Thailand: Evidence from enhanced airborne geophysical data. J. Asian Earth Sci. 107, 12–25.
Shao, C.L., Wang, J.S., Li, Z.J., Liu, W.J., 2015. Study on gold metallogenic belt and mineralization concentrated area of Laos. Mineral Exploration 6 (6), 787–796 (in Chinese with English abstract).
Shi, M.F., Lin, F.C., Liu, C.J., Li, X.Z., Wang, H., 2013. Classification and metallogenesis of metallogenic belts in Southeast Asia and the neighbouring southwestern part of China. Sedimentary Geology and Tethyan Geology 33 (2), 103–112 (in Chinese with English abstract).
Smith, S., Olberg, D., Manini, T., 2005. The Sepon gold deposits, Laos: exploration, geology and comparison to Carlin-type gold deposits in the Great Basin (abstract). In Geological Society of Nevada Symposium, Nevada, pp. 899–915.
Sone, M., Metcalfe, I., 2008. Parallel Tethyan sutures in mainland Southeast Asia: New insights for Palaeo-Tethys closure and implications for the Indosinian orogeny. C. R. Geoscience 340, 166–179.
Sutherland, F.L., Bosshart, G., Fanning, C.M., Hoskin, P.W.O., Coenraads, R.R., 2002. Sapphire crystallization, age and origin, Ban Huai Sai, Laos age based on zircon inclusions. J. Asian Earth Sci. 20, 841–849.
Tabakh, M.E., Utha-Aroon, C., 1998. Evolution of a Permian carbonate platform to siliciclastic basin: Indochina Plate, Thailand. Sed. Geol. 121, 97–119.
Thanh, N.X., Tu, M.T., Itaya, T., Kwon, S., 2011. Chromian-spinel compositions from the Bo Xinh ultramafics, Northern Vietnam: Implications on tectonic evolution of the Indochina block. J. Asian Earth Sci. 42, 258–267.
Thanh, N.X., Hai, T.T., Hoang, N., Lan, V.Q., Kwon, S., Itaya, T., Santosh, M., 2014. Backarc mafic–ultramafic magmatism in Northeastern Vietnam and its regional tectonic significance. J. Asian Earth Sci. 90, 45–60.
Wang, H., Wang, J.L., Chen, M.T., Wang, J.Y., Shi, M.F., Zhu, H.P., 2014a. Geological characteristics and prospecting index of the PhuKham Cu-Au deposit in Xiangkhouang province, Laos. Contributions to Geology and Mineral Resources Research 29 (1), 66–71 (in Chinese with English abstract).
Wang, J.H., Yin, A., Harrison, T.M., Grove, M., Zhang, Y.Q., Xie, G.H., 2001. A tectonic model for Cenozoic igneous activities in the eastern Indo-Asian collision zone. Earth Planet. Sci. Lett. 188, 123–133.
Wang, Q.F., Deng, J., Li, C.S., Li, G.J., Yu, L., Qiao, L., 2014b. The boundary between the Simao and Yangtze blocks and their locations in Gondwana and Rodinia: Constraints from detrital and inherited zircons. Gondwana Res. 26, 438–448.
Wang, S.F., Mo, Y.S., Wang, C., Ye, P.S., 2016. Paleotethyan evolution of the Indochina Block as deduced from granites in northern Laos. Gondwana Res. 38, 183–196.
Wang, X.M., Shi, Y.J., 2016. Geological characteristics and prospecting derections of lateritic gold deposits in Pangkuam Cu-Au miningarea of Laos. Mineral Resources and Geology 30 (2), 193–197 (In Chinese with English Abstract).
Ward, S.H., 1971. Induced polarisation methods in mineral exploration. Geoexploration 9 (2–3), 79. (https://doi.org/10.1016/0016-7142(71)90049-4).
Xia, X.P., Nie, X.S., Lai, C.K., Wang, Y.J., Long, X.P., Meffre, S., 2016. Where was the Ailaoshan Ocean and when did it open: A perspective based on detrital zircon U-Pb age and Hf isotope evidence. Gondwana Res. 36, 488–502.
Yan, D.P., Zhou, M.F., Wang, C.Y., Xia, B., 2006. Structural and geochronological constraints on the tectonic evolution of the Dulong-Song Chay tectonic dome in Yunnan province, SW China. J. Asian Earth Sci. 28, 332–353.
Yin, A., 2010. Cenozoic tectonic evolution of Asia: A preliminary synthesis. Tectonophysics 488, 293–325.
Zhang, J.J., Zhong, D.L., Zhou, Y., 1999. Tectonic Evolution of Southeast Asia and the Ailao-Honghe Tectonic Belt. Geological Review 454 (4), 337–344 (in Chinese with English abstract).
Zhang, R.H, Zhang, B.H., Liu, X.C, Che, L.K., 2012. Tectonic deformation characteristics and the control on ore in B. Phatem gold deposit in Bak-ou county, Luang Pracang province of Laos. Contributions to Geology and Mineral Resources Research 27(3), 341-348 (In Chinese with English Abstract).
Zhao, Y.P., He, G.C., Lu, J.H., 2013. Geological characteristics and metallogenic model of typical Au ore deposit in Laos. Mineral Resources and Geology 27(Sup.), 41-46 (In Chinese).
Zhao, Z.X., Wang, Z.C., Zhu, Y.Z., Yan, C.M., 2015. Copper mineral resources and metallogenic prediction in Laos. Geology and Resources 24 (3), 237–241 (In Chinese with English Abstract).
Zhou, J.X., Huang, Z.L., Zhou, M.F., Zhu, X.K., Muchez, P.Z., 2014. sulfur and lead isotopic variations in carbonate-hosted Pb-Zn sulfide deposits, southwest China. Ore Geol. Rev. 58, 41–54.
Zhou, J.X., Luo, K., Wang, X.C., Wilde, S.A., Wu, T., Huang, Z.L., Cui, Y.L., Zhao, J.X., 2018a. Ore genesis of the Fule Pb-Zn deposit and its relationship with the Emeishan Large Igneous Province: Evidence from mineralogy, bulk C-O-S and in situ S-Pb isotopes. Gondwana Res. 54, 161–179.
Zhou, J.X., Wang, X.C., Wilde, S.A., Luo, K., Huang, Z.L., Wu, T., Jin, Z.G., 2018b. New insights into the metallogeny of MVT Pb-Zn deposits: A case study from the Nayongzhi in South China, using field data, fluid compositions, and in situ S-Pb isotopes. Am. Mineral. 103, 91–108.
Zhou, J.X., Xiang, Z.Z., Zhou, M.F., Feng, Y.X., Luo, K., Huang, Z.L., Wu, T., 2018c. The giant Upper Yangtze Pb-Zn province in SW China: Reviews, new advances and a new genetic model. J. Asian Earth Sci. 154, 280–315.
Zi, J.W., Cawood, P.A., Fan, W.M., Wang, Y.J., Tohver, E., McCuaig, T.C., Peng, T.P., 2012. Triassic collision in the Paleo-Tethys Ocean constrained by volcanic activity in SW China. Lithos 144–145, 145–160.
Zou H.J., Hu R.Z., Liu M.Q., Huang J.G., Ren T. Wu Jin., 2017. Enlightenment, exploration practice and suggestions from the geotectonic evolution of the Southeast Asian mainland to the prospecting directions in Northern Laos. Acta Mineralogica Sinica 37 (supl. 1), 894-895 (In Chinese).